



Norwegian
Meteorological Institute
met.no

met.no report

no. 16/2009
Oceanography

Iceberg modeling at met.no: Validation of hindcast experiment

Göran Broström, Arne Melsom, Ana Carrasco
Norwegian Meteorological Institute

Title

Iceberg modeling at met.no: Validation of hindcast experiment

Section

Oceanography

Author(s)

Göran Broström

Arne Melsom

Ana Carrasco

Client(s)

StatoilHydro

Abstract

The present study is a part of an effort to implement the Canadian Hydraulics Centre (CHC) iceberg model in the Norwegian Meteorological Institute (met.no) operational system. One important part of the implementation plan is to validate the system against observations. The validation is separated into two parts: i) a validation of the current model that is used to force the drift of the icebergs; this study is presented here, and ii) a validation of the iceberg drifts using available observations of iceberg trajectories. The second validation study is presented in an accompanying study (Broström et al., 2009). Atmospheric and wave forcing will be validated elsewhere.

In this study we show that the underlying hindcast ocean model reproduces data in a satisfactory way. Most of the discrepancies may be attributed to energetic eddy field and the associated problems in modeling an eddy field, and the tidal currents, correct in space and time. The mean and statistical quantities show good agreement with data, and the model reproduces statistical quantities in a satisfactory way. However, it is also shown that the model does not reproduce the observations accurately in time. Here we suggest that that this is due to i) some error in tidal forcing (i.e., the data and model has slightly different peaks in the power density spectrum), and ii) a possible time lag between model and observations.

Keywords

Validation, ocean model, iceberg model

Date

21122009

Report no.

16

Classification

Free Restricted

ISSN 1503-8025

e-ISSN <nummer>

Client's reference

Contract 4501431719

Disiplinary signature

Lars Petter Røed (sign)

Responsible signature

Øystein Hov (sign)

Executive summary

The present study is a part of an effort to implement the Canadian Hydraulics Centre (CHC) iceberg model in the Norwegian Meteorological Institute (met.no) operational system. One important part of the implementation plan is to validate the system against observations. The validation is separated into two parts: i) a validation of the current model that is used to force the drift of the icebergs; this study is presented here, and ii) a validation of the iceberg drifts using available observations of iceberg trajectories. The second validation study is presented in an accompanying study (Broström et al., 2009). Atmospheric and wave forcing will be validated elsewhere.

In this study we show that the underlying hindcast ocean model reproduces data in a satisfactory way. Most of the discrepancies may be attributed to energetic eddy field and the associated problems in modeling an eddy field, and the tidal currents, correct in space and time. The mean and statistical quantities show good agreement with data, and the model reproduces statistical quantities in a satisfactory way. However, it is also shown that the model does not reproduce the observations accurately in time. Here we suggest that that this is due to i) some error in tidal forcing (i.e., the data and model has slightly different peaks in the power density spectrum), and ii) a possible time lag between model and observations.

List of content

EXECUTIVE SUMMARY	3
1 INTRODUCTION.....	5
1.1 REGIONAL DESCRIPTION.....	5
1.1.1 <i>Origin of icebergs</i>	5
1.1.2 <i>Main current systems and hydrography</i>	7
1.3 AIM OF STUDY	9
2 HINDCAST FOR 1987-1988.....	10
2.1 ATMOSPHERIC MODEL AND DATA.....	10
2.2 OCEANIC MODEL AND DATA.....	11
2.3 WAVE MODEL AND DATA	12
3 MEAN FIELDS.....	14
3.1 TEMPERATURE FIELDS.....	14
3.2 ABSOLUTE VELOCITY FIELDS.....	14
4 TEMPERATURE AND CURRENTS AT POINT POSITIONS	17
4.1 RIG BARH_S4	17
4.1.1 <i>Model-observation comparison</i>	19
4.2 OTHER CURRENT RIGS	30
5 RELEASE OF ICEBERGS.....	35
5.1 FRANZ JOSEF LAND ICEBERGS.....	35
5.1.1 <i>Releases south of Franz Josef Land</i>	35
5.1.2 <i>Releases south-southwest of Franz Josef Land</i>	36
5.1.3 <i>Releases east of Franz Josef Land</i>	37
5.1.4 <i>Releases southeast of Franz Josef Land</i>	38
5.1.5 <i>Releases north of Franz Josef Land</i>	39
5.2 RELEASES IN SVALBARD AREA.....	40
6 RESULTS AND DISCUSSION.....	42
6.1 SUMMARY FOR VALIDATION FROM IDAP MOORINGS	42
6.2 SUMMARY FOR ICEBERG MOVEMENTS	42
6.3 FINAL COMMENTS	43
REFERENCES.....	44
APPENDIX.....	47

1 Introduction

There are several icebergs each year in the Barents Sea. The icebergs pose a threat to shipping and off-shore industries and it is desirable to be able to forecast iceberg motions in the Barents Sea to increase safety of marine operations. Furthermore, it is valuable to have a model tool to investigate the statistical properties, such as iceberg distributions and iceberg sizes, in the Barents Sea for more accurate risk predictions regarding shipping and oil and gas exploration. The results from risk predictions may also be used for designing equipments to be used in Barents Sea.

As of today, the most comprehensive iceberg model is probably the model developed at the Canadian Hydraulics Center (CHC) (Kubat et al., 2007; Kubat et al., 2005), which is also used operationally at the Canadian Ice Service (CIS) and the International Ice Patrol (IIP). A version of this model is also being used to determine iceberg movements in the vicinity of oil rigs at Grand Banks and provides a guide for decisions on the towing of icebergs. To implement a modeling capability for iceberg geometry and iceberg drift in the Barents Sea the present project aims to incorporate the CHC iceberg model into the operational system at met.no. A significant part of the project is to validate the iceberg model for 1987-1988: the underlying physical forcing is analyzed in the present study while the iceberg model validation is presented in an accompanying report (Broström et al., 2009). The latter report also contains additional information on the iceberg model.

1.1 Regional description

The overall aim of the project is to implement an iceberg modeling capability in the Barents Sea; the goal is both to implement a semi-operational model and to be able to perform sensitivity studies for iceberg distribution in the Barents Sea. Accordingly it is useful to give a short description of the geographical aspects regarding icebergs, and the regional oceanography that are important for the drift of icebergs. A map of the Barents Sea showing some important glaciers producing icebergs for the present domain is given in Fig. 1.1.

1.1.1 Origin of icebergs

The most important glaciers that form the icebergs found in the Barents Sea are outlined in Fig. 1.1. A brief description is outlined below:

1. Franz Josef Land is an archipelago that contains 191 ice-covered islands. The main part of large icebergs detected in Barents Sea probably originates from Franz Josef Land (Spring, 1994). Notably, the Franz Josef Land glaciers produce a relatively steady stream of icebergs and the most important is
 - a. Renown Glacier at Wilzek Land: Probably the largest producer of large icebergs in the Barents Sea (Spring, 1994).
2. There are some glaciers on Svalbard that produce iceberg that reaches the Barents Sea. The Svalbard glaciers have a history of short episode surges rather than producing a steady stream of icebergs. The most important for the Barents Sea are

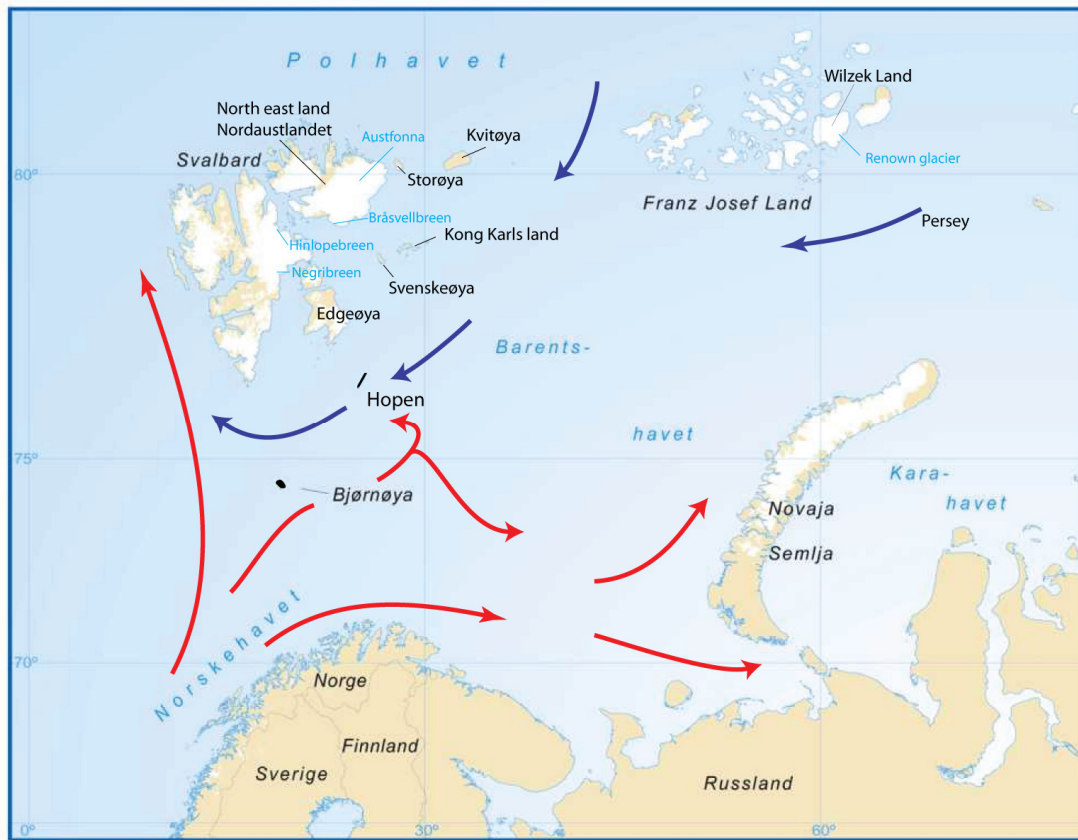


Figure 1.1: Map of the Barents Sea area. Blue text corresponds to glaciers that are important producers of icebergs for the Barents Sea. Red arrow represents warm currents while blue arrow represents cold currents.

- a. Bråsvellbreen: Lies on the Nordaustland and is a part of the Austfonna glacier. This outlet is about 1100 km² and it is grounded in water along a 30 km long glacier front. It surged in 1936-38 (Liestøl, 1969) and the front advanced up to 20 km during the surge (Schytt, 1969).
- b. Negribreen: Surged in 1935-36 and advanced about 12 km in less than a year along a 15 km long section of the front, with an average speed of 35 m d⁻¹ (Liestøl, 1969).
- c. Hinlopbreen: Surged in 1970 and calved about 2 km³ of icebergs in a single year (Hagen et al., 2003; Liestøl, 1973).

For 1987-1992 (the years of the IDAP study, see Spring, (1994) or Broström et al. (2009)) it seems reasonable to assume that most icebergs originated from Franz Josef Land (Spring, 1994). However, the large number of icebergs during 1988 was probably from a glacier surge; it is not known which glacier that surged and, accordingly, the Svalbard glaciers cannot be ruled out.

1.1.2 Main current systems and hydrography

The Barents Sea is a shallow marginal sea with a maximum depth of about 500 m (Fig. 1.2). Due to the rotation of the earth (or more exact due to conservation of potential vorticity), ocean currents tend to flow along depth contours when the stratification is weak (LaCasce, 2000; Nøst & Isachsen, 2003; Walin, 1972). Accordingly, we expect that topography will play an important role in the Barents Sea. However, it should be recognized that baroclinic effects are also important for certain flow structures. For instance, there is a flow of about 1-3 Sv ($1 \text{ Sv} = 10^6 \text{ m}^3 \text{ s}^{-1}$) of warm water through the Barents Sea (Schauera et al., 2002), which keeps the main part of the Barents Sea open during winter.

Starting from south we have the current system moving northwards off of the Norwegian coast: this current system constitutes of the open ocean Norwegian Atlantic Current (NwAC) and the Norwegian Coastal Current (NCC). When reaching the opening of the Barents Sea, a certain part of the NwAC enters the Barents Sea, the remainder travels along the steep topography toward Svalbard (also creating a sharp front north of Bjørnøya between the Norwegian Sea and the Barents Sea).

There are at least two different branches that enter the Barents Sea. Along the northern Norwegian coast flows the North Cape Current (NCaC) that progresses along the coast and becomes the Murmansk Coastal Current (MCC). One branch of the MCC proceeds into the Kara Sea while the other branch moves northwards along Novaya Zemlya in the eastern Barents Sea. There is also an inflow of warm water into the Barents Sea north of the NCaC in the Bjørnøya Trench and the Hopen trench (Ingvaldsen, 2005; Ingvaldsen et al., 2004). Here, a significant part travels along depth contours in the Hopen trench and there is a return flow on the northern branch of the trench (Skagseth, 2008).

The flows described above are directed northward and eastward. There are also important southward and westward flows of cold water, which carry the icebergs during their movements in the Barents Sea. Starting from the east, the Persey current is an inflow of water from the Arctic and the Kara Sea between Novaya Zemlya and Franz Josef Land. The Persey current flow in a western direction south of Franz Josef Land and will thus carry icebergs from Franz Josef Land westward. There is also an inflow of water between Franz Josef Land and Svalbard (Kwok et al., 2005). These waters are typically cold; however, as they are also fresh they tend to be buoyant and are located in the upper ocean. The current move westward south of Svalbard over the shallow areas around Hopen and Bjørnøya, i.e., on the Spitsbergen bank. It should be noted that a relatively large number of grounded icebergs can be found in this area (Spring, 1994). There is an exchange of water between the cold water close to Franz Josef Land and Svalbard, and the interior of the Barents Sea; however, we have not found any quantitative analysis of the importance of this process. As a final comment on the Barents Sea current system, south of the Hopen and Bjørnøya islands there is a deep trench. On the southern side of this trench there is a warm eastward flowing current as mentioned earlier, however, this current follow the topography and thus turn northward and westward when reaching the Barents Sea central bank (Skagseth, 2008). Accordingly, we may have a relatively warm current moving westward south of the Hopen and Bjørnøya islands.

Besides the ocean currents, sea ice is also important for the iceberg dynamics. Not only does sea ice affect the atmospheric circulation due to its strong impact on the air-sea heat flux, but also by decreasing the wave amplitude (Broström & Christensen, 2008; Squire, 2007; Squire et al., 1995): furthermore, sea ice is also very important for the balance of forces that act on an iceberg (Lichey & Hellmer, 2001; Savage, 2007). In fact, it takes only a relatively minor ice thickness and ice concentration for the ice to trap the iceberg, which thus starts to move with

the ice (Lichey & Hellmer, 2001; Savage, 2007). Much of the ice in the Barents Sea comes from the Arctic Ocean (Kwok et al., 2005; Løset & Carstens, 1996). According to Kwok et al. (2005) the mean winter ice volume import in the passage between Svalbard and Franz Josef Land passage is 40 km^3 . However, over a period 10 years (between 1994-2003), variability of the ice area and volume import is high and volume import ranges from -280 km^3 to 340 km^3 . The direction of ice import between Svalbard and Franz Josef Land is controlled by the location of the atmospheric low in the Barents Sea. The magnitude is determined by two factors: the strength of wind forcing and the availability of thick multi year (MY) ice near the passage. The second factor is connected to the large-scale location of the Perennial Ice Zone (PIZ) within the Arctic Ocean (Kwok et al., 2005). It is likely that these factors are affected by the large scale atmospheric flows, which in turn are correlated with the North Atlantic Oscillation (NAO) index¹. This is for instance visualized in the correlation of the heat flux and the NAO index; furthermore, the ice covered area may change by 20-30% due to changes in weather patterns as associated with the NAO index (Furevik, 2001). In any case, we may conclude that the overall sea ice drifts is southwestward from Franz Josef Land toward the area south of Svalbard where icebergs finally melt.

In the present study, our main interest is the general advection path for the icebergs, which is along the south-westward drift from Franz Josef Land toward the region south of Svalbard (Keghouche et al., 2007; Spring, 1994). The stranding of icebergs in the shallow area between Hopen and Svalbard is also a solid observation which is of significance in the present context. Further discussions on iceberg climatology for the Barents Sea can be found elsewhere (Abramov, 1992; Zubakin et al., 2004; Zubakin et al., 2005).

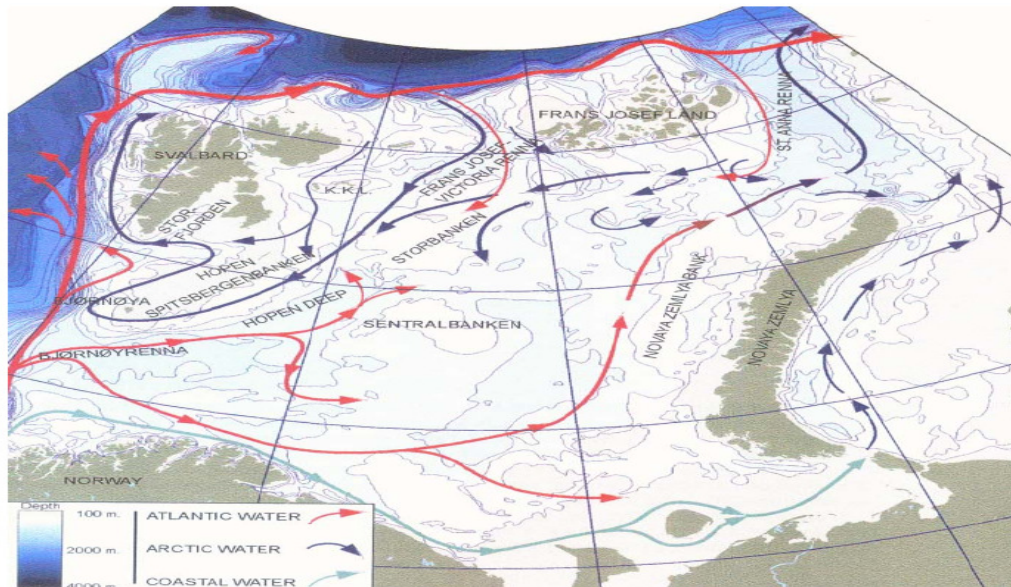


Figure 1.2: The main current systems in the Barents Sea (Keghouche et al., 2007).

¹ The NAO may have different definitions but it is usually defined as the pressure difference between Iceland and Lisbon or the Azores. NAO is a measure on the typical tracks of the low pressure systems over North Atlantic Ocean on monthly time scales and beyond.

1.3 Aim of study

The overall aim of the project is to develop an iceberg model for the Barents Sea that can be used for:

1. Hindcasting movements of icebergs in the Barents Sea.
2. Risk predictions for the iceberg presence in the Barents Sea area.
3. Enabling a forecast system for icebergs in the Barents Sea.

To achieve these goals it is important to validate the model system to ensure that it gives reasonable results. The present study focuses on the underlying models systems (atmosphere, wave, ocean and ice models) that provide forcing for the iceberg model. The validation of the iceberg model is described elsewhere (Broström et al., 2009)

The remainder of this document is organized in sections as follows:

- Short description of the model systems.
- Analysis of the basic model fields.
- Validation of temperature and current data for specific points.
- Outline of the general advection pathways of icebergs in the Barents Sea.
- Discussion of the general results from this study.

2 Hindcast for 1987-1988

To force the iceberg model we need data on

1. Atmospheric wind (in principle we also need air temperature and solar radiation; however in the present model air temperature is approximated with the sea surface temperature, and a fixed solar radiation is accurate enough for the present purpose).
2. Ocean currents and temperature (mainly upper 50 m).
3. Significant wind-wave height, significant swell-wave height and swell direction.

For the present study we aim at a hindcast for the period August 1987-August 1988, and the data we use to force the model are described below. It should be noted that the hindcast data are not fully consistent with each other as the atmospheric fields were not used to force the ocean/ice model; neither were the ocean, ice, and wave fields allowed to influence the atmospheric model.

2.1 Atmospheric model and data

The atmospheric hindcast run was based on the ECMWF ERA40 reanalysis (<http://www.ecmwf.int/research/era/do/get/era-40>) and was downscaled using the Hirlam v.6.4.2 numerical weather prediction model (Undén et al., 2002). The model has 248×400 grid points and a horizontal resolution of 0.1 degree. 40 levels are used in the vertical, the model domain is shown in Fig. 2.1. Compared to the ERA40 dataset, the downscaling using HIRLAM with ~10 km horizontal resolution, generally improves the 10 m wind speed in the whole HIRLAM10 domain. ERA40 is continuously underestimating 10 m wind speed at coastal areas and also for land stations. At the stations around Svalbard, there is a net overestimation of the wind speed in both ERA40 and HIRLAM, but high speeds are not overestimated neither by ERA40 nor by HIRLAM10 (Haakenstad, personal communication). We do not consider any validation of the atmospheric model as this will be presented elsewhere within the Norwegian Deepwater Programme Metocean Project. However, given that the atmospheric model is based on a well documented hindcast analysis, we expect that the atmospheric model will provide reliable forcing for the iceberg model (note that wind is generally not one of the most important factors for icebergs drift; it mainly influences the drift of icebergs through the ocean currents, the drift of sea ice, and by setting up a wave field).

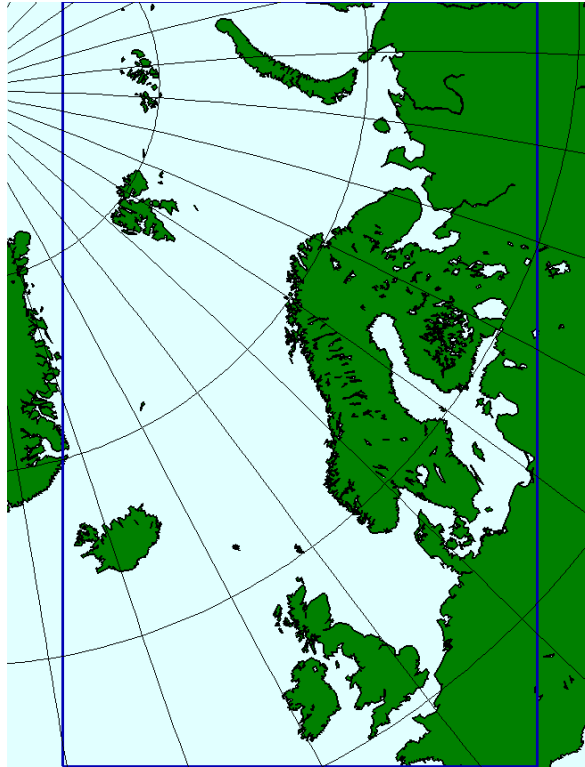


Figure 2.1: Model domain for HIRLAM10 (within blue frame). The model relies on the global ERA-40 forcing/reanalysis fields for boundary conditions and forcing.

2.2 Oceanic model and data

To produce fields for hydrography and currents for the period August 1987 to August 1988 we used a coupled numerical ocean-ice model. The ocean code (Meteorological Institute Princeton Ocean Model, MI-POM) is a local version of the Princeton Ocean Model (POM) (Blumberg & Mellor, 1987) modified for operational use at the Norwegian Meteorological Institute (Engedahl, 1995). MI-POM is a three-dimensional baroclinic primitive equation model with sigma (terrain-following) coordinates in the vertical. The model includes a 2.5-order turbulent mixing scheme (Mellor & Yamada, 1982). Ice dynamics is described by Meteorological Institute Ice Model (MI-IM) (Røed & Debernard, 2004). The thermodynamics is modeled with one ice layer that includes fully prognostic treatment of internal energy, ice concentration and ice mass, while the heat capacity of the snow layer is neglected. This treatment is similar to the thick-ice / thin-ice / open-water formulation of (Hibler, 1979) but with a fully conservative treatment of the prognostic total heat content of the sea ice.

The coupled ocean-ice model was set up for the domain shown in left panel of Fig. 2.2, and covers the Barents Sea region and part of the Nordic Seas, with a 4 km horizontal resolution. The atmospheric forcing fields were taken from the ECMWF ERA-40 reanalysis (<http://www.ecmwf.int/research/era/do/get/era-40>). Tidal forcing included eight harmonic constituents (M2, S2, N2, K2, Q1, O1, P1 and K1) gathered from barotropic tidal models (Flather, 1981; Gjevik, 1990). The tidal forcing was applied at the open lateral boundaries. In addition, sea surface temperature (from ERA-40) and merged ice concentration fields (a

combination of data from the ice service of the Norwegian Meteorological Institute and the ERA40 data-set) were assimilated via a nudging scheme (Albretsen & Burud, 2006).

The Barents Sea model ("Iceberg-drift4km") received its lateral boundary values from a coarser coupled ocean-ice model ("Arctic20km" at 20 km resolution) whose domain covers the entire Arctic Ocean and parts of the Northern North Atlantic. The setting up of this coarser model was similar to "Iceberg-drift4km" with the exceptions that this model did not have tidal forcing, and that the lateral boundary values came from climatology.

For this study the outer model (Arctic20km) was run from January 1985 to September 1988 while the inner model (Iceberg-drift4km) from January 1986 to September 1988: The model domain for Arctic20 is shown in the right panel of Fig. 2.2. The actual model fields used for analysis of iceberg drift were limited to the period between August 1987, and August 1988. The ocean model utilized 21 sigma-levels, but the final output fields were interpolated to a set of z -levels (0, 10, 20, 30, 40, 50, 60, 70, 80, 90, 100 and 150 m). The output variables, saved every two hours, were sea surface height, horizontal water velocity, salinity, temperature, ice thickness, ice concentration and ice velocity.

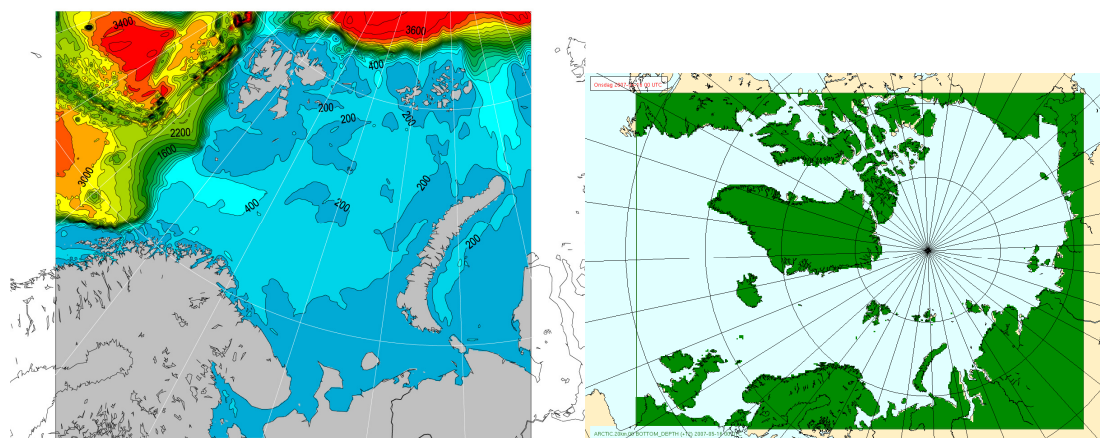


Figure 2.2: Left panel: domain and topography (meters) of "Iceberg-drift4km". Right panel: model domain for Arctic-20km (green)

2.3 Wave model and data

The wave model is based on the WAM model (Cavaleri, 2007; Komen et al., 1994), which predicts the wave energy in different directions for various frequency intervals. The data in this study is taken from the downscaling of the reanalysis as described for the atmospheric model above. The model domain is shown in Fig. 2.3. The 30% ice concentration contour was used as a closed boundary for the wave model. We do not consider any validation of the wave model as this will be presented elsewhere within the Norwegian Deepwater Programme. Although we do not consider a validation of the wave fields here we expect that the wave fields are fairly accurate given that we have confidence in the wind fields (which provides the forcing for the wave model). If wind is described correctly, it is well known that wave models generally provides very reliable results (Cavaleri, 2007; Komen et al., 1994).

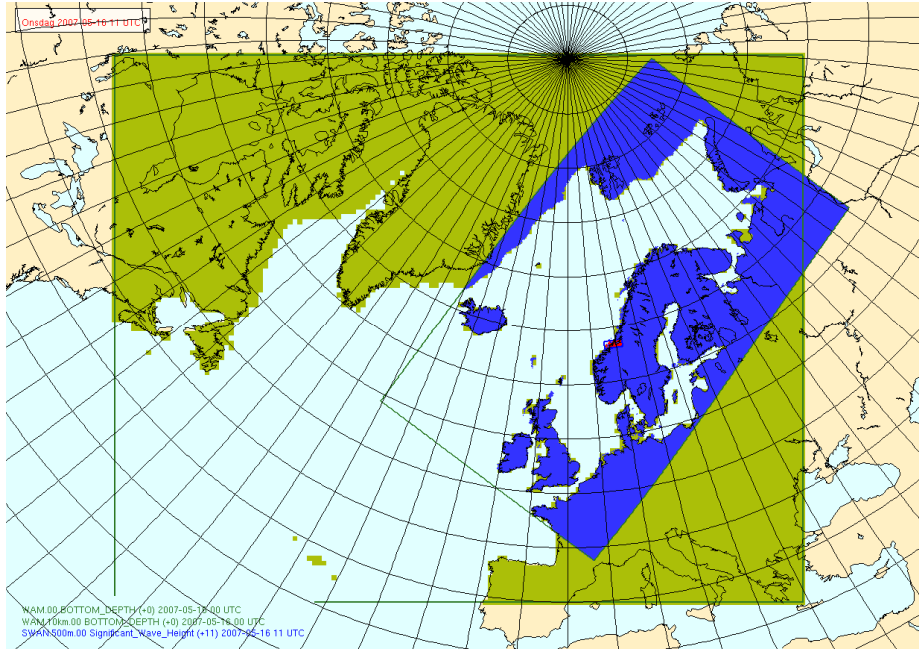


Figure 2.3: Model domains for WAM.50km (green) and WAM.10km (blue)

3 Mean fields

3.1 Temperature fields

The monthly mean sea surface temperature (SST) fields from August 1987 to July 1988 are shown in Fig. 3.1 a, b. As expected the highest temperatures are found in July-September and the coldest in January-March. In the winter months the warm Norwegian Atlantic Current (NwAC) is clearly seen as a warm feature along the continental slope between Lofoten and Svalbard. The inflow of warm water into the southern Barents Sea is also clearly visible as in the figures.

3.2 Absolute velocity fields

The monthly mean absolute velocity fields at the sea surface from August 1987 to July 1988 are shown in Fig. 3.2 a, b. Again the NwAC is clearly seen as high velocities along the continental slope between Lofoten and Svalbard. Somewhat north of Lofoten there is a deeper area stretching out from the central Barents Sea to the continental shelf (i.e., the Hopen Trench or Bjørnøyrenna). Here the monthly mean absolute velocities are weaker and we can spot a current moving into the Barents Sea along the topography in the Hopen trench. The extension of this current east of 30°E is not clear from these set of figures and there appears to be no steady and clear current path from this point. We can also see the Norwegian Coastal Current (NCC) that enters the Barents Sea as high velocities on the coastline of the northern Norway. From the northern tip of Norway, we see some evidence that the current mainly flows eastward although the figures are not conclusive on this matter. On the northern tip of Novaya Zemlya there is a strong current system that is directed eastward. The strong topographic structure of this area suggests that the current is a part of the topographically controlled current loop flowing southward from the Franz Josef Land, eastward north of Novaya Zemlya, and northward northeast of Novaya Zemlya, as is also indicated in Fig. 1.2.

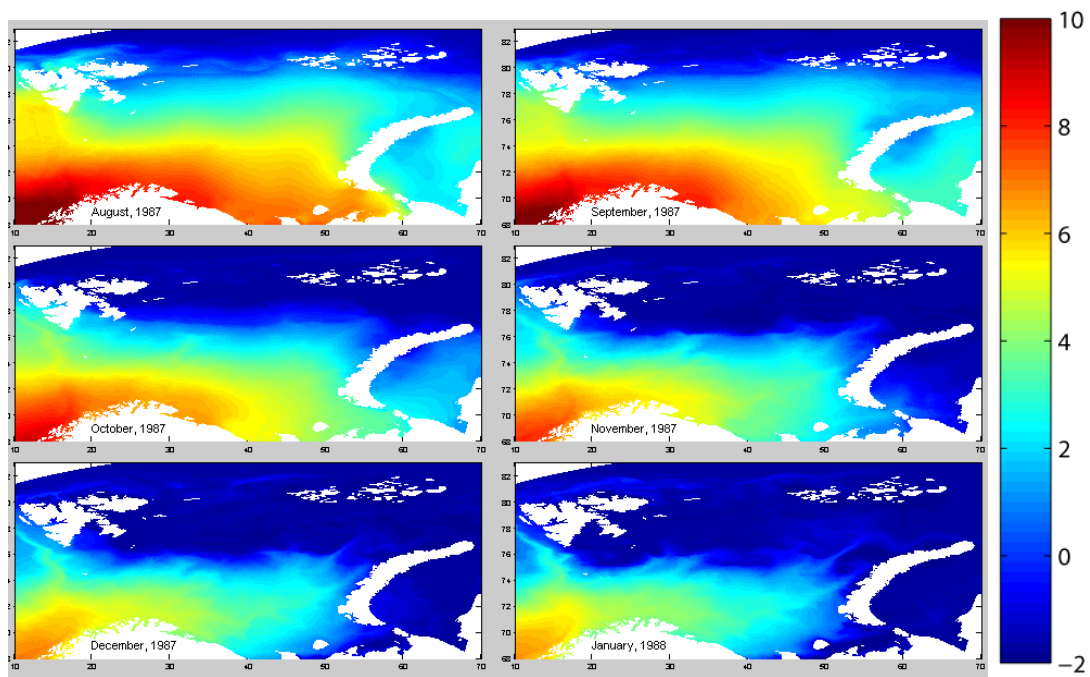


Figure 3.1a: The monthly mean temperature from Aug, 1987 to Jan 1988.

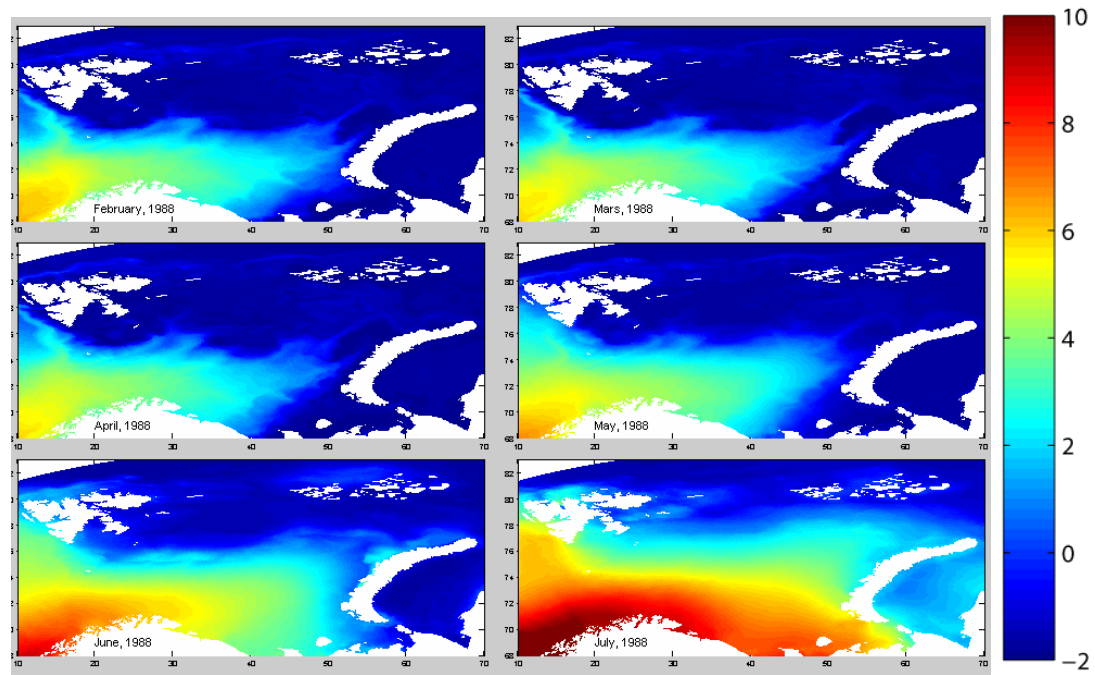


Figure 3.1 b: The monthly mean temperature from Feb, 1988 to July 1988.

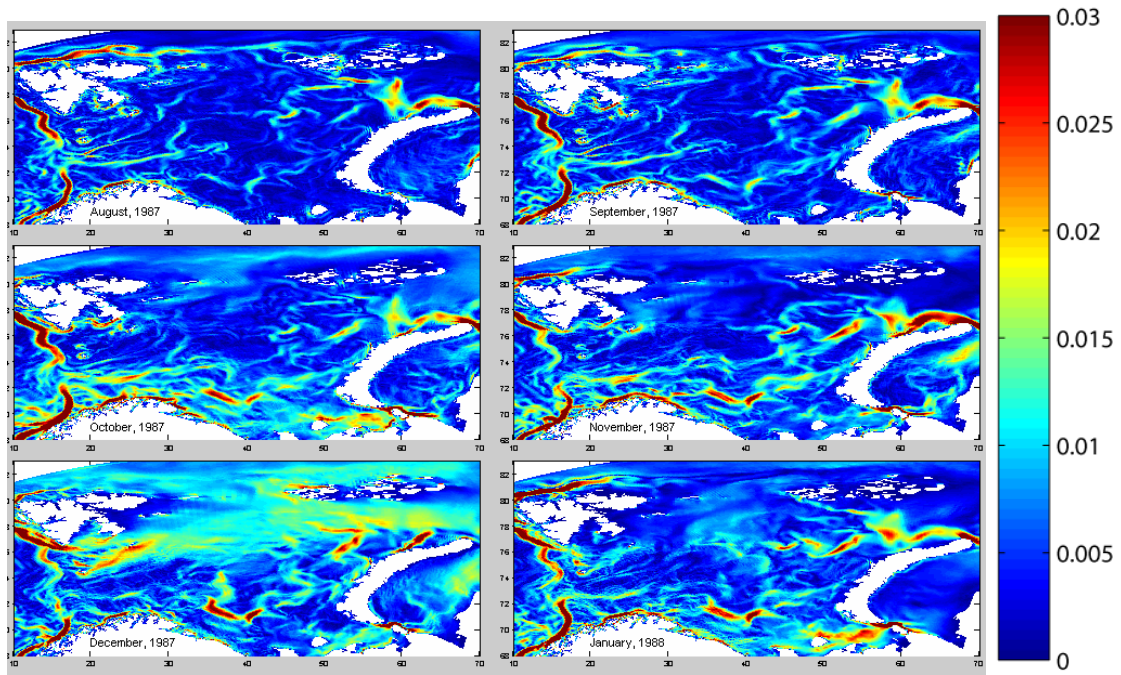


Figure 3.2 a: The monthly mean of the absolute velocity at the sea surface from Aug, 1987 to Jan 1988.

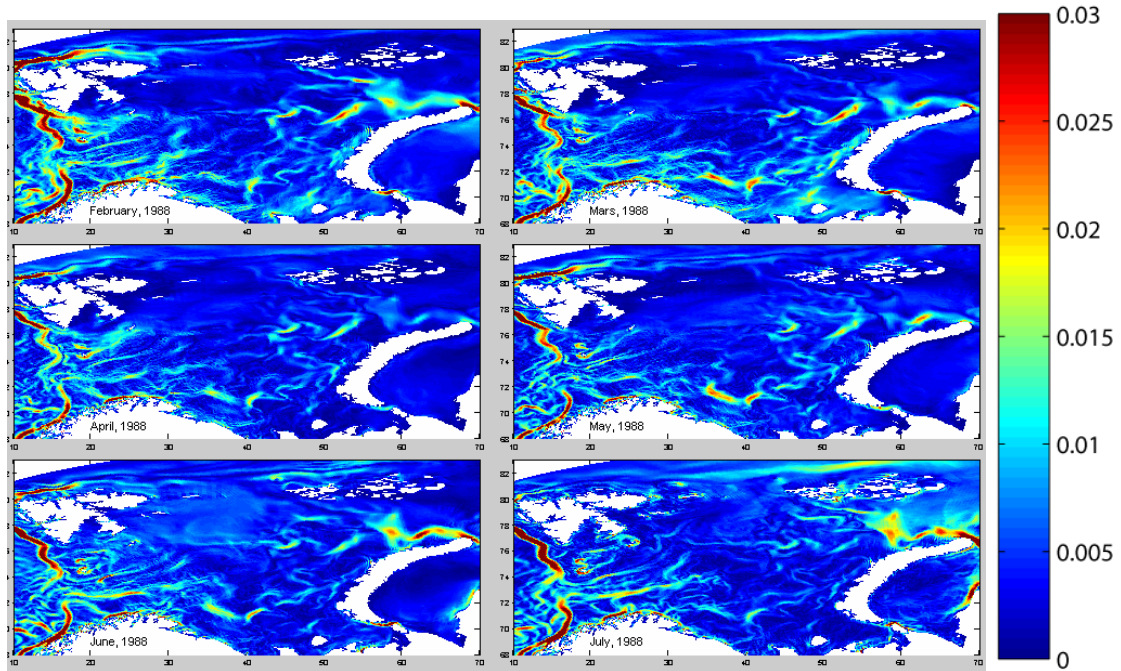


Figure 3.2 b: The monthly mean of the absolute velocity at the sea surface from Feb, 1988 to July 1988.

4 Temperature and currents at point positions

StatoilHydro has kindly provided ocean current observations taken during the IDAP project. The positions of the current rigs are shown in Fig. 4.1 a, b. The area colored in red in Fig. 4.1b is the Hopen trench. The observations were taken at a number of depths and the exact periods with data and depth range of the moorings depend on the location. Given that that the icebergs are generally not more than say 50-100 m deep we will only use the observations in the upper 100 m in this validation study. We consider a number of comparisons and start with plotting the time series for the temperature and the absolute velocity over the model year (August 1987 to August 1988) to visually compare the model with observations. We also consider scatter plots where the observed and modeled current speed for given times are plotted against each other, this is a test of the model's capability of reproducing currents in time. We also display the frequency distribution of the current speed for estimating the capability of the model to reproduce the energetics of the ocean currents. The current direction frequency, $Dir(\theta, t)$, and transport at a given depth, $U_{Dir}(\theta, t)$, in different directions are also investigated. These are defined as

$$Dir(\theta, z) = \frac{1}{T} \int_0^T \delta[\theta'(t, z) - \theta] dt, \quad (4.1a, b)$$

$$U_{Dir}(\theta, z) = \frac{1}{T} \int_0^T U(\theta', t, z) \delta[\theta'(t, z) - \theta] dt,$$

$\delta[\theta' - \theta(t, z)]$ is here given by

$$\delta[\theta' - \theta(t, z)] = \begin{cases} 1 & \text{if } abs(\theta' - \theta(t, z)) \leq \theta_{res} / 2 \\ 0 & \text{if } abs(\theta' - \theta(t, z)) > \theta_{res} / 2 \end{cases} \quad (4.2)$$

where $\theta_{res} = 10^\circ$ is the resolution of the final distribution. The unit of $Dir(\theta, t)$ is deg^{-1} and the unit of the $U_{Dir}(\theta, t)$ is thus $\text{ms}^{-1} \text{deg}^{-1}$. The direction frequency gives the probability for the current to be in a certain direction, the transport direction also takes into account the strength of the velocity in that direction. Notably, the current direction frequency as defined here bears clear resemblance to the use of current roses, which is customary in geophysics. The strength of the definition here is that the current direction frequency from model and observation can be plotted in the same graph for easy comparison. For more detailed model/observation comparisons we interpolate the model results linearly in time to the time of the observations to find a consistent model and observational dataset.

4.1 Rig Barh_s4

We use the rig Barh_s4 (27.1256°E, 75.0411°N) as an example for this study: this rig is one of the northeastern rigs and will probably be one of the rigs that reflect conditions of iceberg infested areas in the best way. The rig is located on a sharp topographic slope on the northern side of the Hopen trench where contours of constant depth are in the west-southwest east-northeast direction. There were observations at 10, 25, 50, 100, 200, and 276 m; however, here we only use the observation in the upper 100 m.

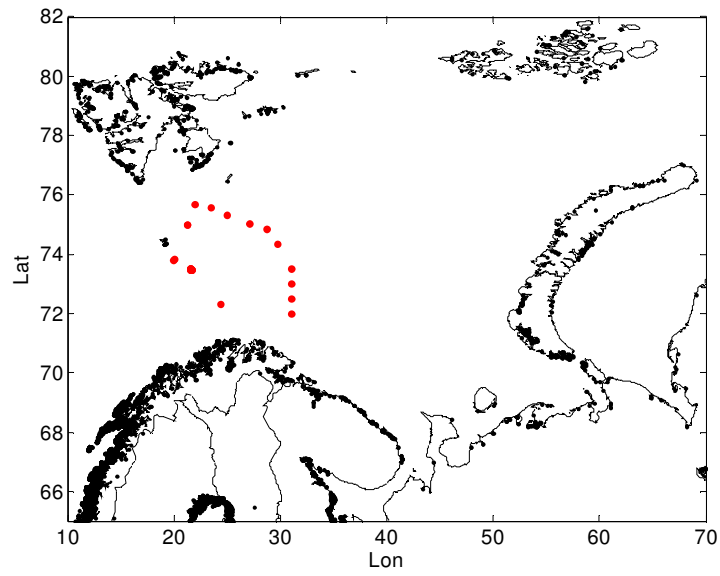


Figure 4.1 a. The positions of the current rigs used in this study.

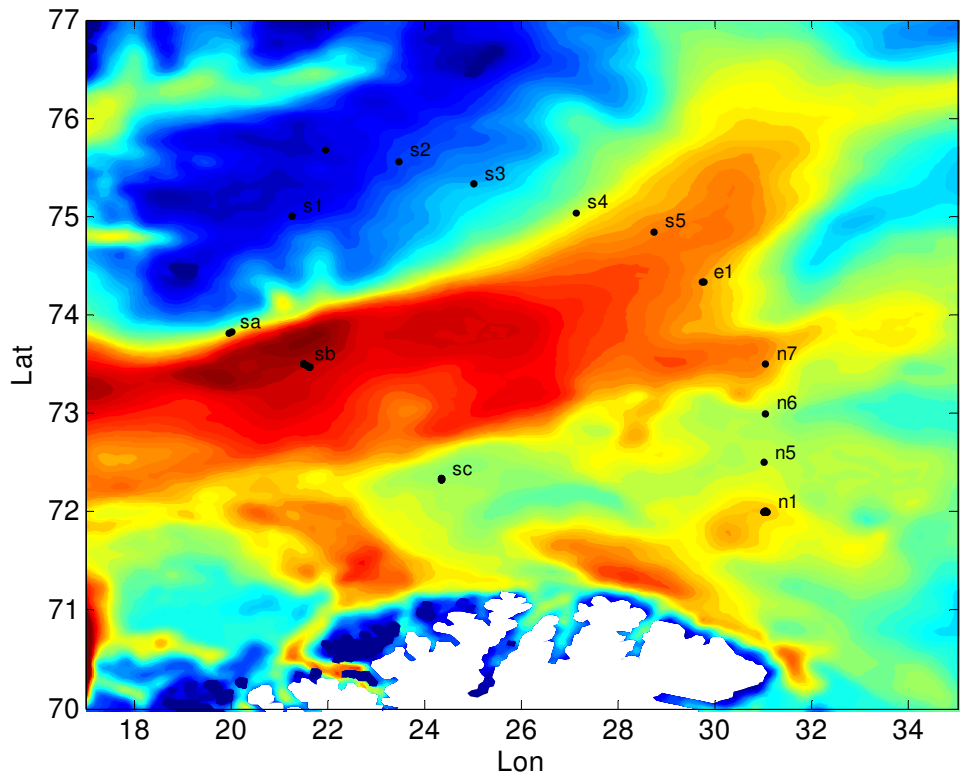


Figure 4.1 b: Blown up figure showing the positions of the current rigs used in this study. Model topography is shown using color mapping. Bjørnøya is located at the dark blue area northwest of rig sa.

4.1.1 Model-observation comparison

Temperature

The temperatures at the four depths are shown in Fig. 4.2. We see that the model temperature is fairly close to observations. One notable feature is that the fluctuations are greater in observation data than in model. However, there are no surface observations in the upper ocean during summer such that we cannot make any statement of the summer temperatures in the surface water. Unfortunately there are few observations of the upper ocean temperature during summer in the IDAP dataset for 1987-1988. However, since sea surface temperature (SST) is assimilated using a nudging technique (Albretsen & Burud, 2006); we expect that upper ocean temperature will be sufficiently correct for this study. However, a more reliable model/data comparison for cold water may be needed for more accurate evaluation of the icebergs melt rates.

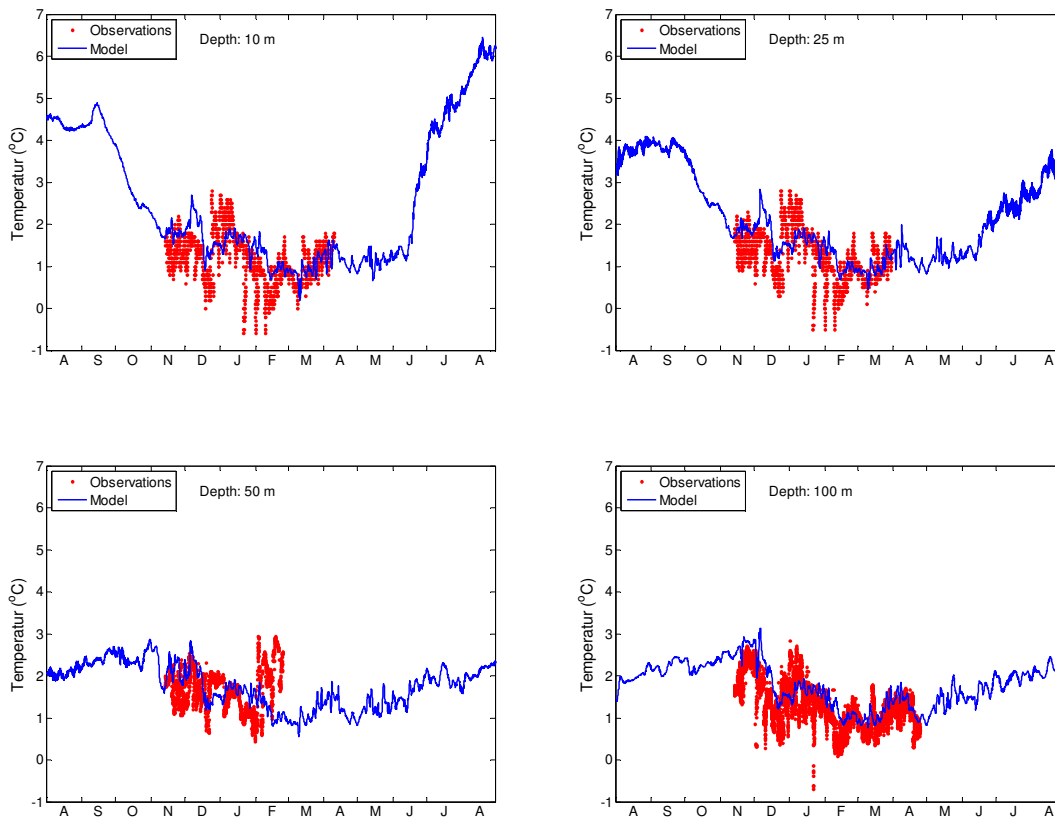


Figure 4.2: The model and observed temperature for rig s4 at 10, 25, 50 and 100 m depth in the upper left, upper right, lower left and lower right panels, respectively.

Absolute velocity

The absolute velocity from observations and model are shown in Fig. 4.3, and a more detailed plot of two different time periods are shown in Fig. 4.4. From Fig. 4.3 it is difficult to make any quantitative statement of the accuracy of the model. However, we can state that the model give predictions that are in the range of the observations although it is not possible to see if they are well correlated in time.

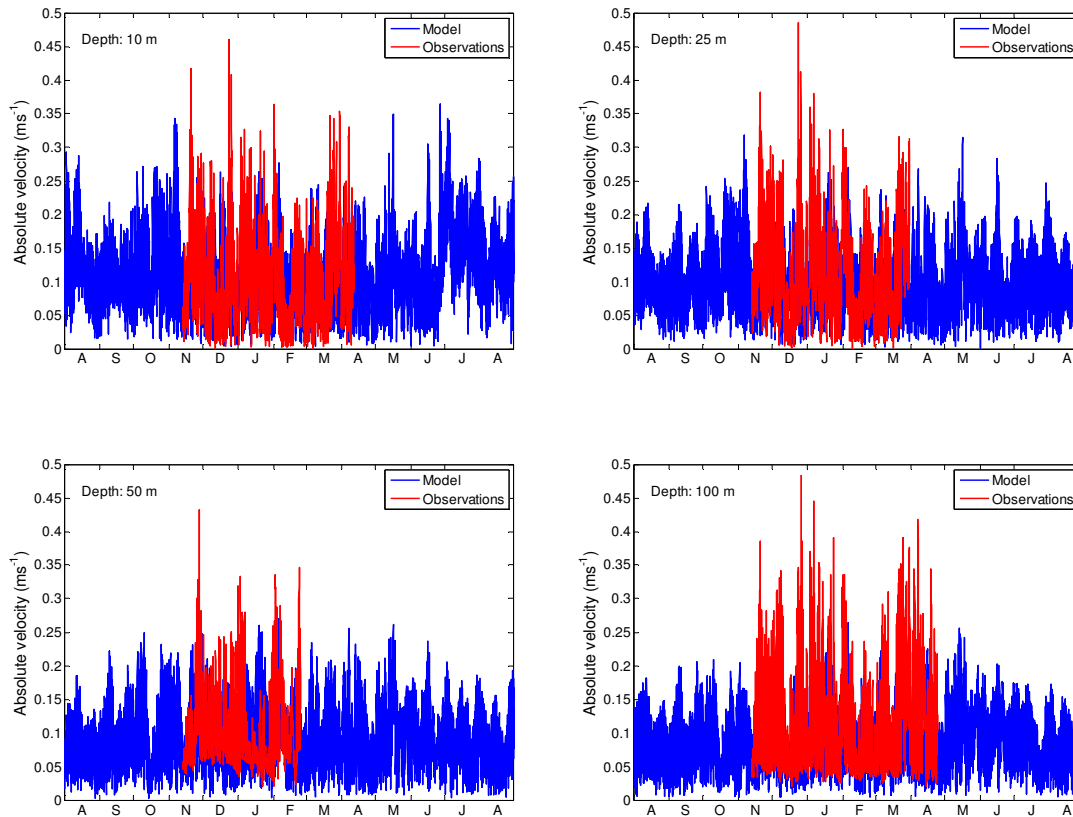


Figure 4.3: The model and observed absolute velocities for rig s4 at 10, 25, 50 and 100 m depth in the upper left, upper right, lower left and lower right panels, respectively.

In order to evaluate any details in how the model reproduces data we show some short periods in Fig. 4.4 a, b. From these figures it is questionable if the model reproduces the observed velocities well in time but shifts from low velocity regimes to higher velocities near the surface seem to be reproduced to some extent. It is not easy to interpret these figures but there are some indications that the oscillating frequencies of the model and the observations are not identical. It should be noted that the observations made from these plots are backed up by power spectral plots presented later. Looking at the “low” velocity positions (i.e., the times with minimum velocity) in Fig. 4.4a the model and observations are out of phase around days 105, 117, 123. They are in phase around days 112,122, and possible around day 130 (this study was based on blow up of these periods but these figures are not shown here). This implies that the phase shift could be about 10%. When investigating on the velocity peaks it looks like there is a small phase shift of a few hours; the observations peak before the model. Turning to Fig. 4.4b, which reflect an early spring situation (i.e., we use the last 30 days of the observation time series) at 100 m depth at station s4 we again see that there is a phase shift between model and observations. Again it is somewhat difficult to make judgment on the reason for the mismatch between model and observations

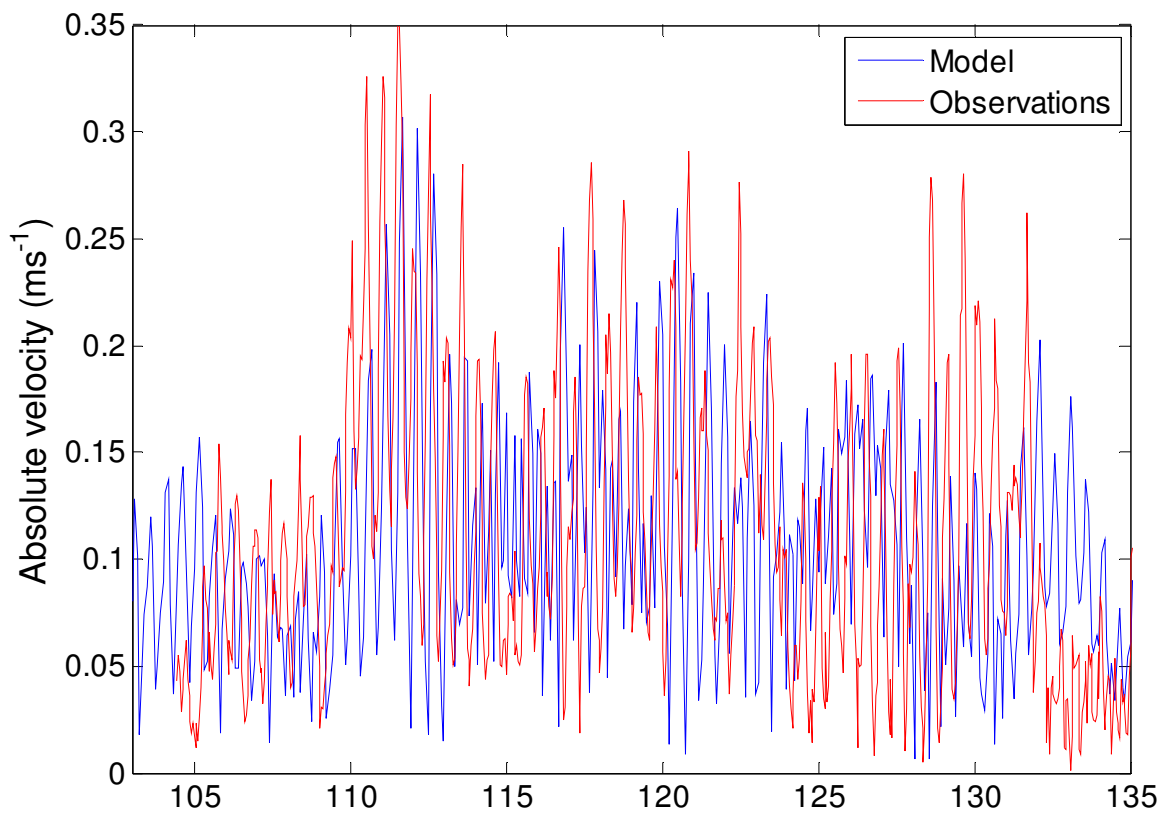


Figure 4.4 a: The model and observed absolute velocities for rig s4 at 10 m depth. This plot shows the period corresponding the first month of observations (i.e., time is days after 1 Aug. 1987).

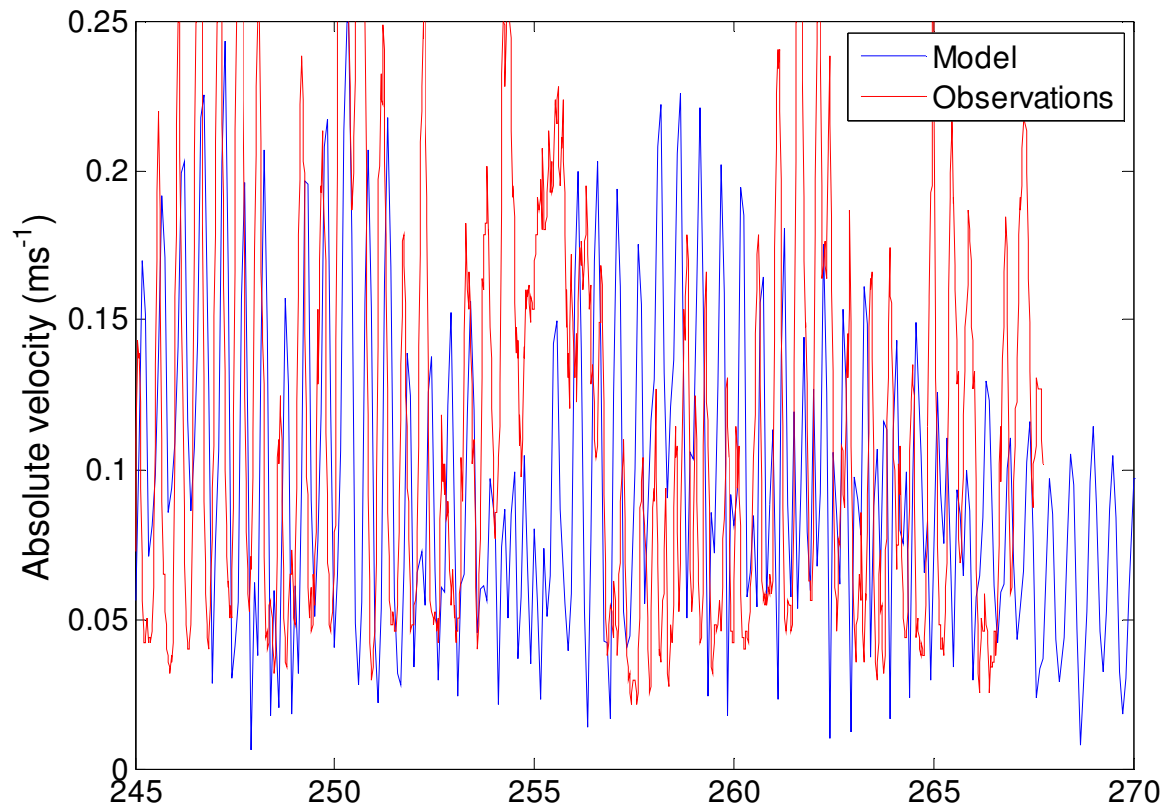


Figure 4.4 b: The model and observed absolute velocities for rig s4 at 100 m depth. This plot shows the period corresponding approximately to April 1988 (i.e., time is days after 1 Aug. 1987).

Velocity-velocity scatter plot

The model output and the time of the observations are generally not simultaneous. Accordingly, to produce the velocity-velocity scatter plot we interpolate the model data to the time of the available observations: the result is shown in Fig. 4.6. We see that there are large scatters in the plots and there are no great correlations between the modeled and observed absolute velocities. From these scatter plots it is also clear that the model has fewer points with high velocities than the observations; furthermore, the model has lower maximum velocities as compared with observations. For 50 and 100 m depths, it also appears that there are very few observations with low velocity, which is also seen in Fig. 4.3. This feature of the observations is questionable.

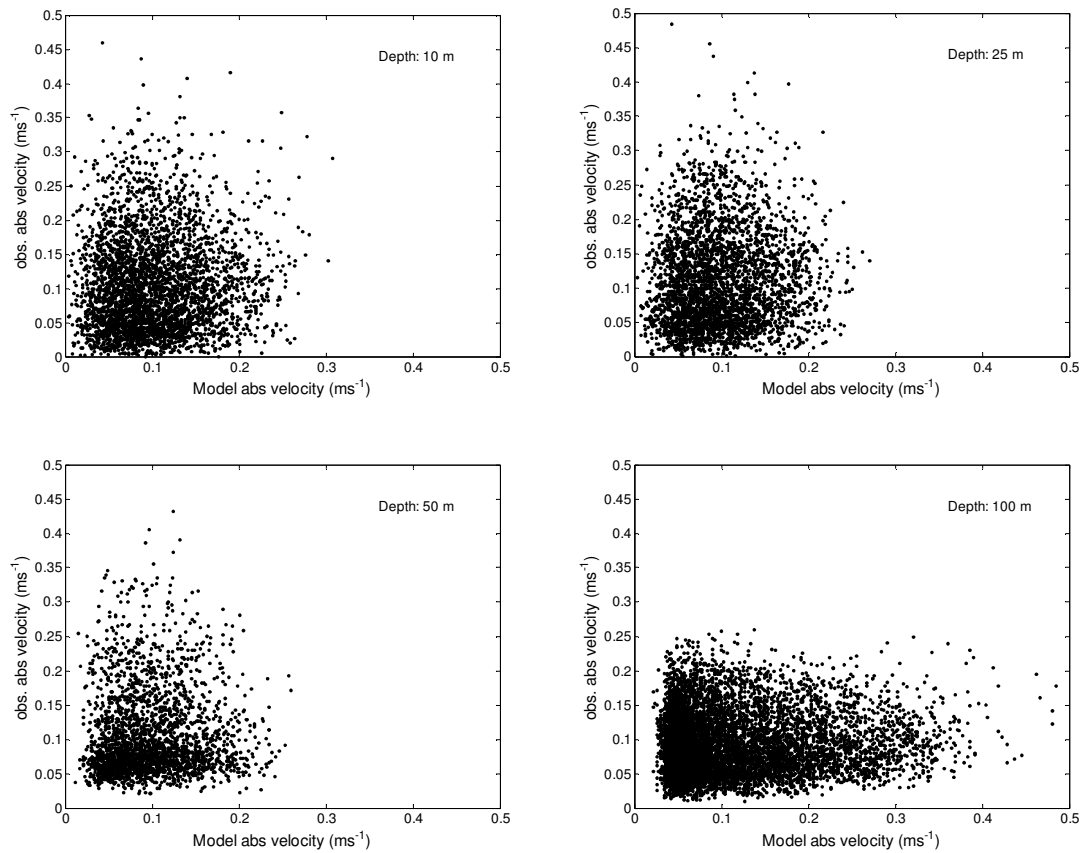


Figure 4.6: Scatter plots of the model and observed (absolute) velocity for rig s4 at 10, 25, 50 and 100 m depth in the upper left, upper right, lower left and lower right panels, respectively.

Velocity frequency

The distributions of observed and modeled velocities are shown in Fig. 4.5. The frequency distribution of the velocities is modeled fairly well. The observed spectrum has a wider distribution and there are more observations with high velocities than predicted by the model, confirming the observations made from the scatter-scatter plots. Again we notice that at 50 and 100 m, there are very few observations with low velocity and there is a peak of observations at low, but not very low, velocity.

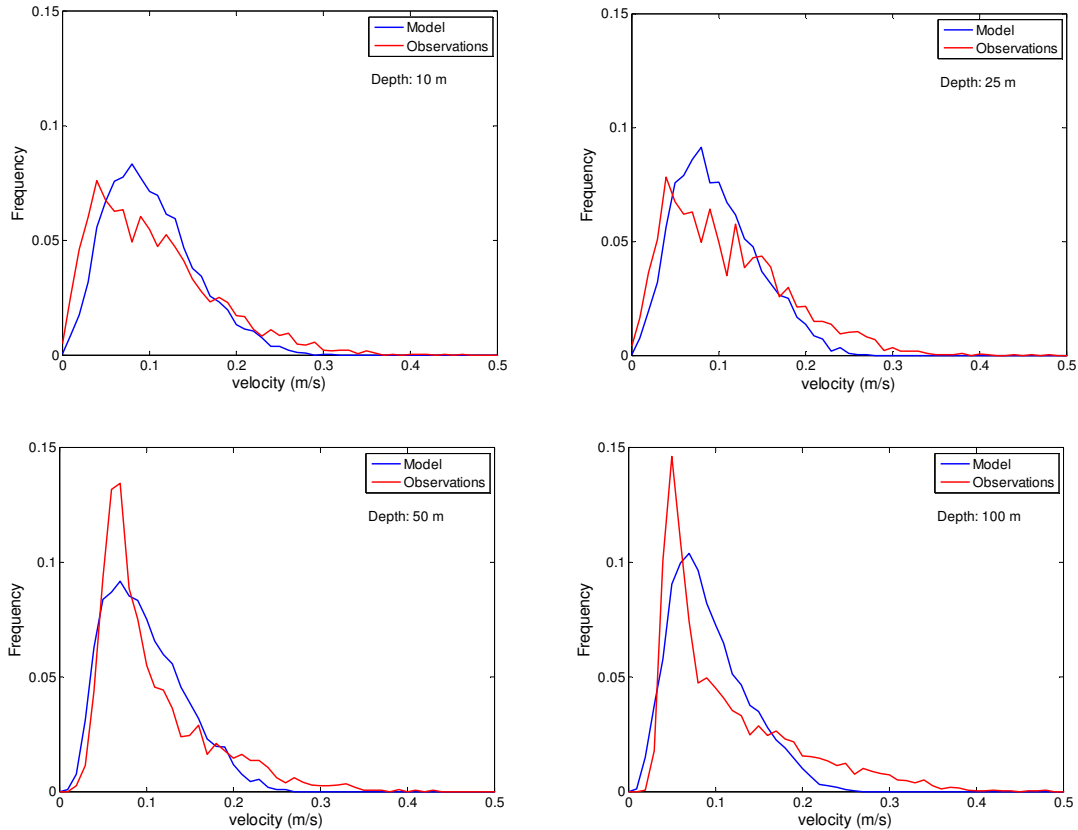


Figure 4.5: The frequency distribution of the model and absolute velocity for rig s4 at 10, 25, 50 and 100 m depth in the upper left, upper right, lower left and lower right panels, respectively.

Direction frequency

One interesting quantity is the (mean) direction of the current. The frequency distributions, calculated according to Eq. 4.1a, of the current direction for different depths are shown in Fig. 4.7. We see a clear peak in current direction in the east-northeast direction with another peak in the west-southwest direction. The position of this current rig is located on the northern side of the Hopen trench and the current direction is consistent with ocean currents following the topography. The model shows a more constant current in the east-northeast direction than indicated by data. Furthermore the model current in the surface water is directed more toward north than observations. Note that the model shows the same main direction for all depths while observations are more northward in the upper part of the water column than in the deeper part.

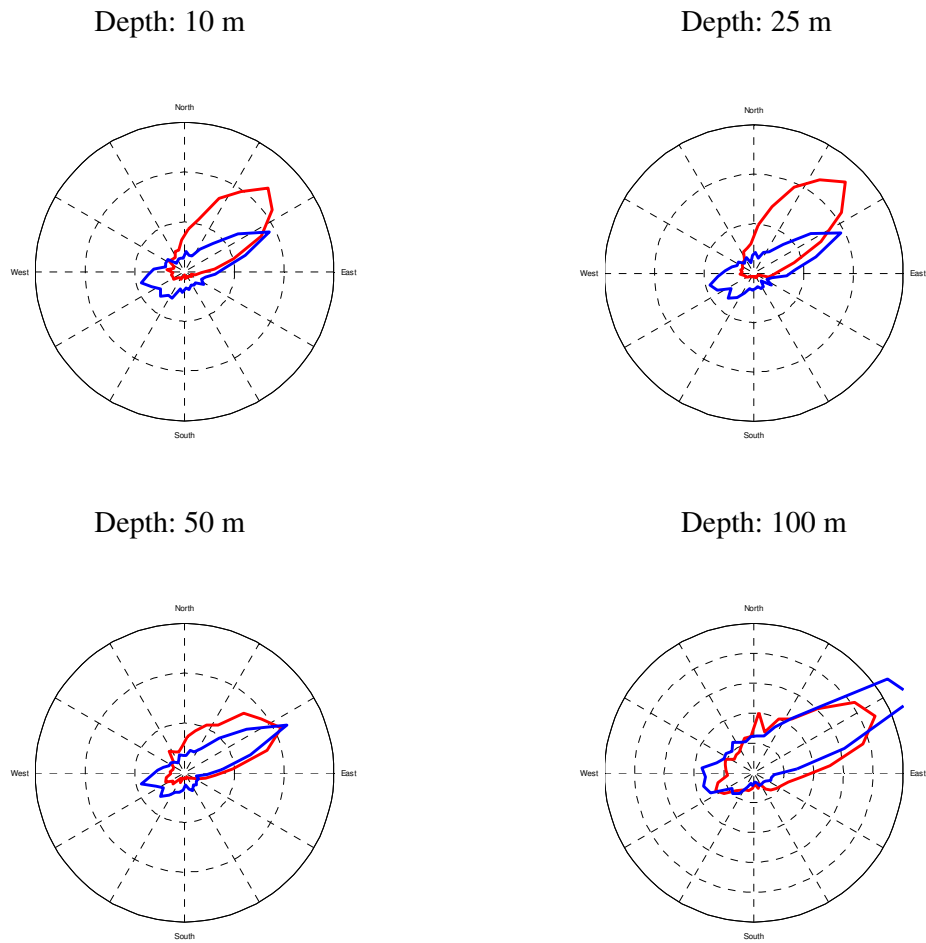


Figure 4.7: The frequency distribution of the model and observed current directions (arb. units) for rig s4 at 10, 25, 50 and 100 m depth in the upper left, upper right, lower left and lower right panels, respectively. Red is for observations and blue is for model.

The transport in different directions

In last subsection we showed the directional distribution. Here we show the integrated transport in different directions, calculated according to Eq. 4.1b, at a certain depth (i.e., the plot shows the mean velocity in a certain direction at the depth of the current meter and bear strong resemblance to a current rose). We argue that this quantity is a better measure of transport, and thus of icebergs movements, than directional frequency as it also accounts for current speed. The plots, Fig. 4.8, are fairly similar to the directional distribution, the main difference is the mass transport, in both model and observations, is more aligned with the topography and it is more directed towards east northeast than the directional distribution.

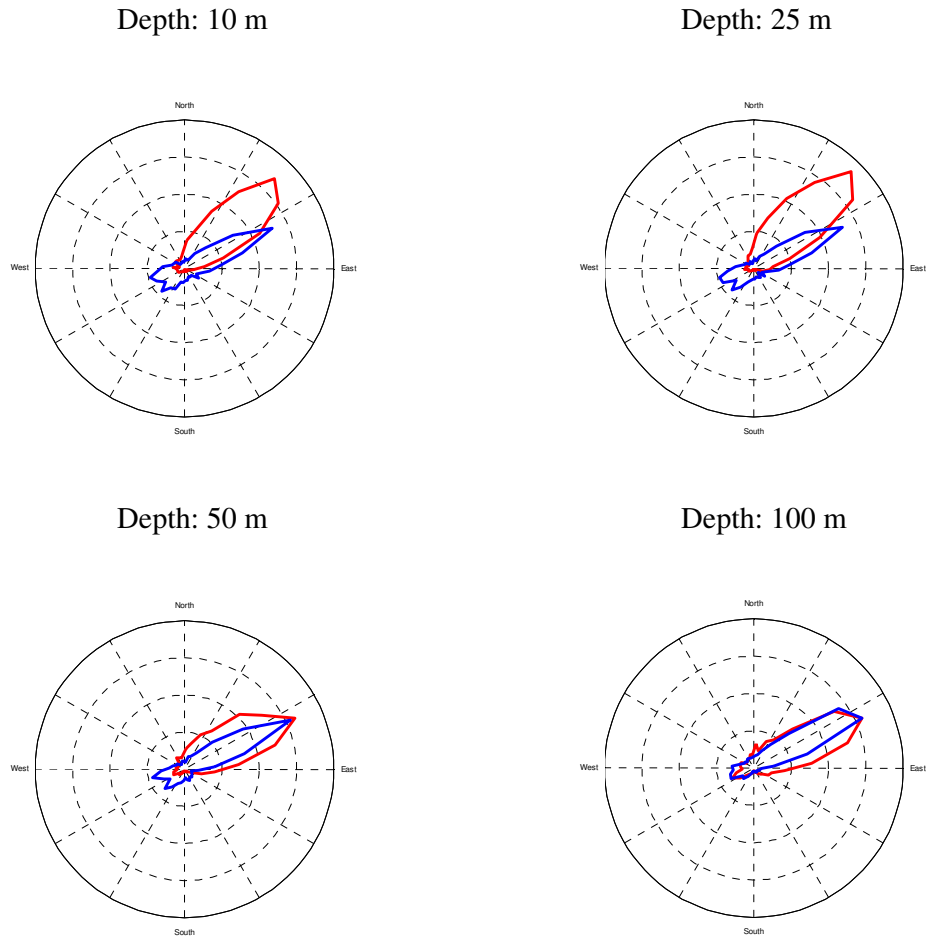


Figure 4.8: The distribution of the model and observed mass transport directions (arb. units) for rig s4 at 10, 25, 50 and 100 m depth in the upper left, upper right, lower left and lower right panels, respectively. Red is for observations and blue is for model.

Why are velocities from model and observation not well correlated?

In above subsections we have shown that many of the statistical features, such as frequency distributions of absolute velocity, current direction and directional transport, are well represented in the model. Nevertheless the scatter-scatter plot, Fig. 4.5, shows that the velocities are not well correlated in time. To further investigate this question we consider i) the possibility that the velocity time series are lagged in time, and ii) that the spectral components are not similar.

In the original data analysis we interpolate the model results to the time of the observations: to test the possibility that there is a systematic time lag between model and observations we consider a test where we interpolate model results from a time $t+\Delta t$ to the time t of the observations. When this has been done we calculate the correlation coefficient for the absolute velocity. By changing time shift, Δt , we calculate the cross-correlation, i.e., the correlation as a function of Δt . The result for 10 m depth at rig s4 is shown in Fig. 4.9, and we see that the maximum correlation takes place for a time lag of $\Delta t=-0.13$ days (or $\Delta t=0.4$ days but this value is further away from $\Delta t=0$ days) while the correlation is much smaller for $\Delta t=0$ days. We also see that the correlation has a sinusoidal shape with a characteristic time scale of 0.52 days (1.92 cycles per day), consistent with semidiurnal tidal water.

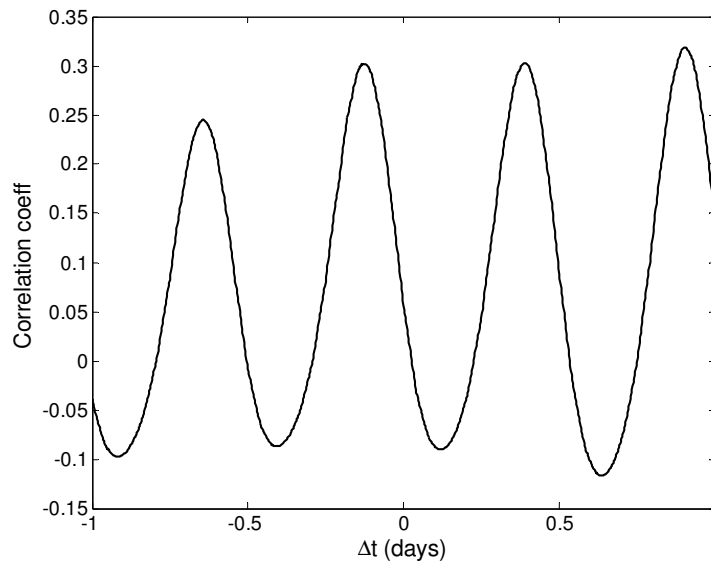


Figure 4.9: The correlation in a scatter-scatter diagram for absolute velocity at 10 at station s4 as a function of shift in the model time series.

The correlation increases for a certain time lag when comparing model with data. It is thus of some interest to see how great the improvement is, thus, we use the case for 10 m depth at station s4 as an example. The original scatter-scatter plot is shown on left panel of Fig. 4.10 while the scatter-scatter plot after application of a time lag of $\Delta t=-0.13$ days is shown on the right panel. We see that the spread is smaller, but still leaves room for significant improvement. Moreover, by using more stations we notice that the time lag is not the same at different stations (not shown) indicating that there is no systematic time lag between data and model, although most stations have an optimal time lag between -0.2 and 0 days.

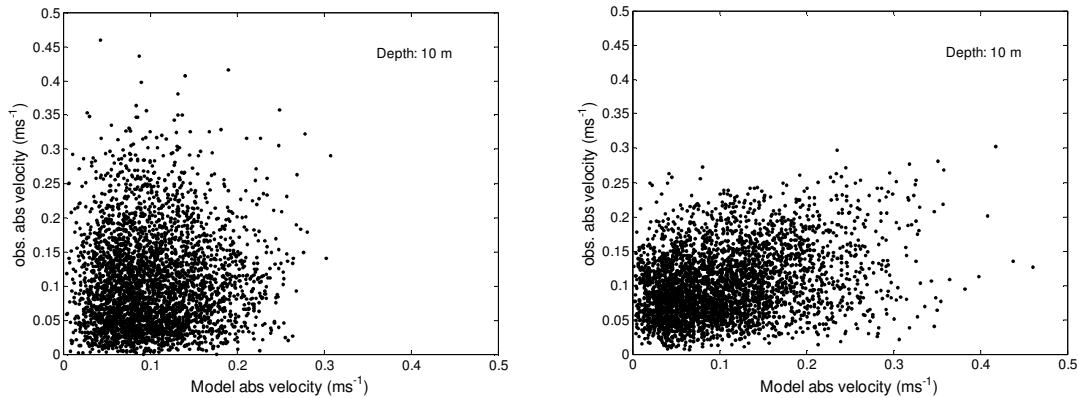


Figure 4.10: The scatter-scatter plot for model and observations from 10 m depth at station s4. Left panel is for zero time lag in the analysis (i.e., it is the same plot as displayed in Fig.4.4 upper left panel), right panel is for a time lag of $\Delta t = -0.1$ days. Note added in proof, the axes are shifted in right panel

Spectral analysis

One other possibility to explain the large mismatch in the scatter-scatter plot is that the model and observations have different characteristic frequencies. Accordingly, we show the power spectral density from 10 m depth at station s4 in Fig. 4.11a. We see that observations exhibit a strong peak for the semidiurnal cycle, consistent with the dominant M2 tide and the inertial currents at the area (note that the inertial frequency is $1.93 \text{ cycles day}^{-1}$ in agreement with the peak frequency found in Fig. 4.11). The model also has a peak around the inertial frequency but the peak is much wider. From the observations on the absolute velocities Fig. 4.4a we did speculate that there may be a phase difference between model and observations of 10%, and this disagreement in frequency comes out from this analysis as well. Similar analysis for different depths and stations indicate that this behavior is not typical for this station but represent an overall feature of the model-observation comparison. The data show a stronger peak in the power spectrum while model shows a wider less intense peak: at some stations the model shows energies at higher frequencies while at other stations it has some energy at lower frequencies. We thus conclude that one of the reasons for the mismatch between model and data in the scatter-scatter point may be due to slightly different frequencies for the absolute velocity components. The reason for this remains unclear. The power spectral density for depth 100 at station s4 is shown in Fig. 4.11b. At this depth the difference in frequencies disappears and the model agrees well with data.

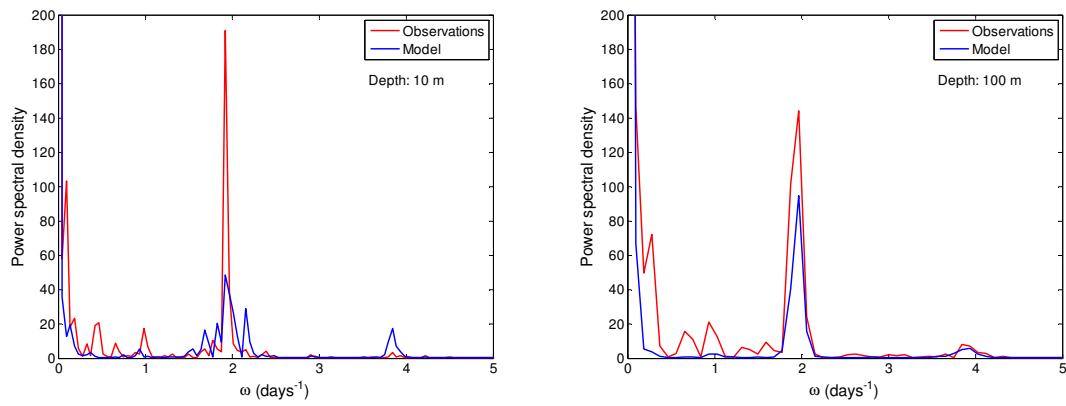


Figure 4.11: The power spectral densities for absolute velocity from model and observations from 10 m depth (left panel) and 100 m depth (right panel) at station s4.

4.2 Other current rigs

The analysis presented above has been repeated for all current rigs and all observational depths above 100 m. At some positions model currents were not available at the largest current meter depths, probably due to an inaccurate representation of topography in the model. For these cases we used data from the lowest grid point with model results. We start with a validation of a more eastern position, e1, and subsequently show results from the northernmost positions s1 to s5. However, all 33 plots from this analysis are shown in the appendix.

Rig e1

Rig e1 is located on the eastern side of the Hopen trench. It is the southernmost station discussed here and accordingly has the strongest signal in the upper ocean temperature (here 3 m), see Fig. 4.12. The model is somewhat colder than the observations but overall there is a good agreement between model and observations. The current in the surface is about 0.1 m/s with a few spikes up to 0.3 m/s. Again the model current is not well correlated with observed velocities although the frequency distribution is similar: the model is somewhat more energetic than the observations but lacking the very highest velocities. The direction of the velocity vector is toward northeast and follows the topography. There is a good agreement between model and observation for the direction of the current, and the model vs. observational transports in different directions also compares favorably.

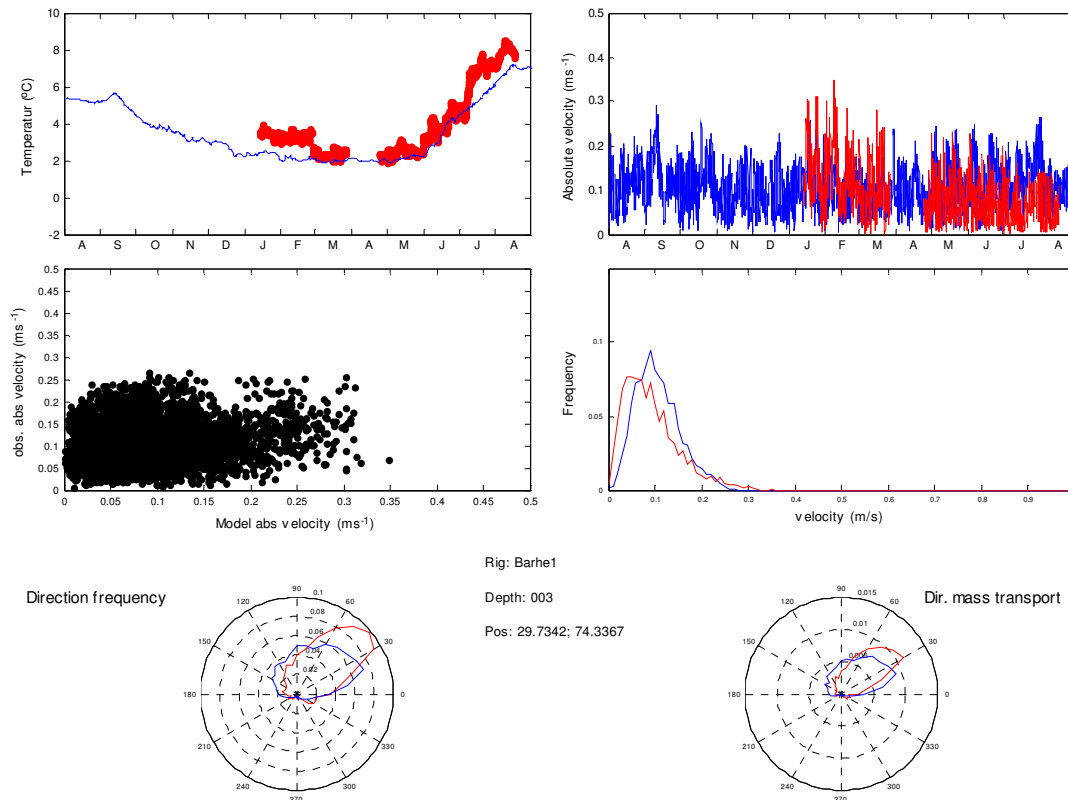


Figure 4.12: Results from current rig Barh_e1 at 3 m.

Rig s1

The station s1 is located up on the shallow section north of the Hopen Trench and somewhat northeast of Bjørnøya. It is characterized by low temperatures and strong currents, Fig. 4.13. The observed temperatures are consistently lower than $-1.95\text{ }^{\circ}\text{C}$. With a salinity of about 35 psu this would be below the freezing point. Accordingly, we conclude that there must be some error in this dataset. Notably, very low and steady temperatures can be found for several locations. The frequency spectrum shows that this is an area of strong (tidal) motions and it has the strongest velocities of all of the stations. Further, the velocity distribution, directional distribution and velocity directional distribution are all very similar between model and observations. The scatter-plot shows that the model results do correlate relatively well with observations in time; however, there is room for improvement in agreement with results from most other stations. Notably, there is a timescale on order one month in the absolute velocity. This could be the spring-neap cycle in the tidal forcing but this is unclear at the moment.

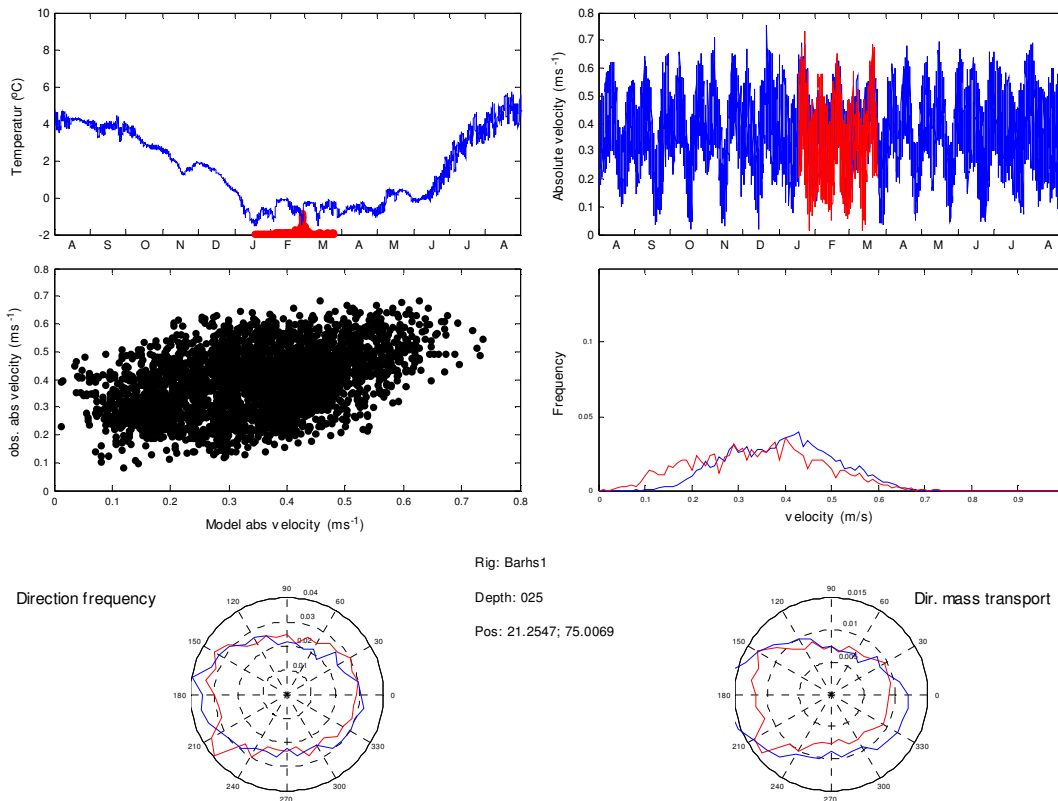


Figure 4.13: Results from current rig Barh_s1 at 25 m.

Rig s2

The current rig s2 is located on a relatively shallow area northeast of s1, and model and observational data from 50 m depth are shown in Fig. 4.14. The topographic steering is not easily detected in Fig. 4.1, it appears to be weak and in west-eastward direction (there is a local west-eastward topographic feature embedded in the general southwest-northeast topographic steering). The observed temperatures are again questionable with very low temperatures. However, the initial part of the time series may be correct in this case, indicating that the model possibly has too high temperatures. The velocity frequency peak is found at a somewhat high velocity in the model results, but the directional frequency and velocity directional frequency are well reproduced by the model. The scatter-plot again shows that currents are not well reproduced in time. Again we see the changes in the absolute velocity with a period of one month. Notably, this is less distinct at some times and more distinct at other times.

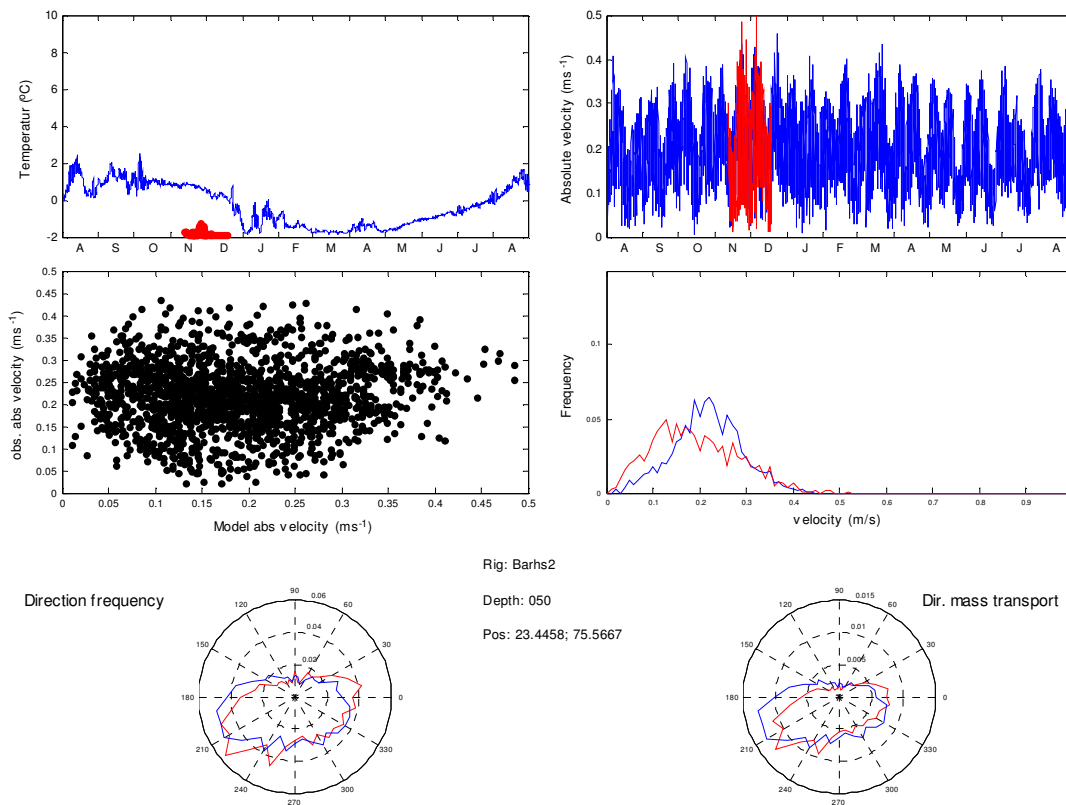


Figure 4.14: Results from current rig Barh_s2 at 50 m.

Rig s3

The current rig s3 is east-southeast of s2, and results from 50 m depth at this station are plotted in Fig. 4.15. Topography steering is again hard to detect from Fig. 4.1 but a north-south topographic slope is likely. The temperature is somewhat high while current statistics agree well between model and data. The model is slightly too energetic. Observations display oscillations over a one month period but it is not as distinct as in the model.

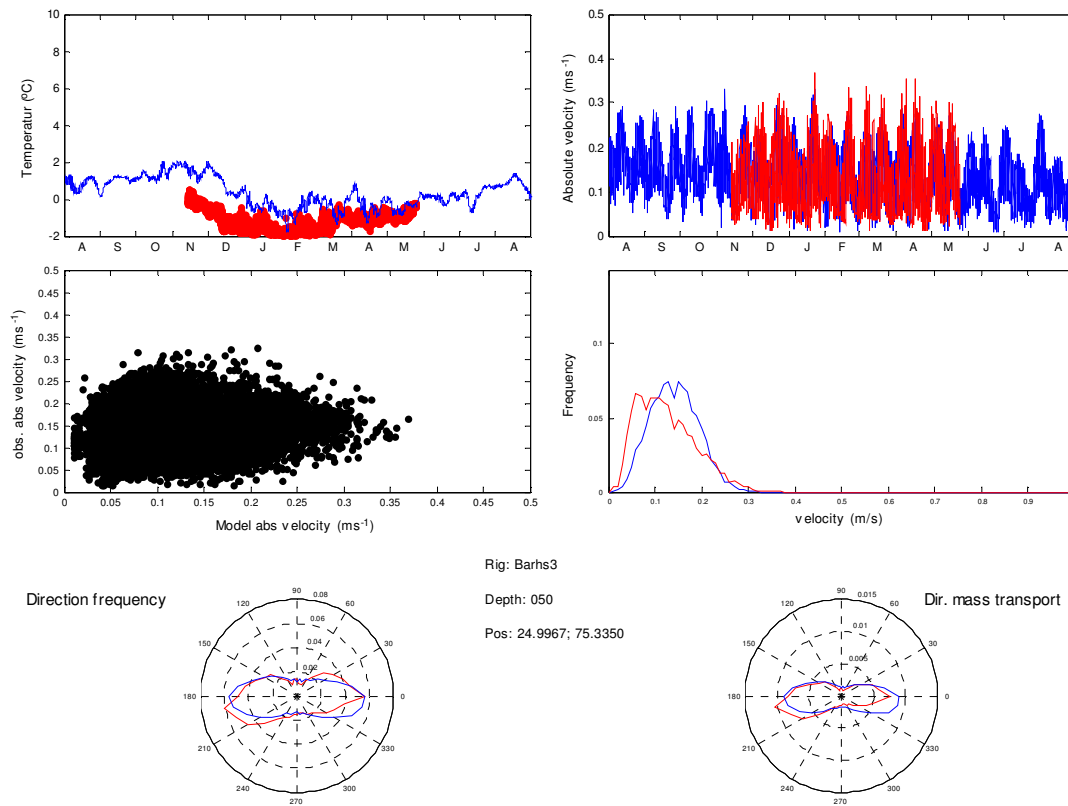


Figure 4.15: Results from current rig Barh_s3.

Rig s5

S5 is located near the centre of the eastern part of the Hopen trench and on a location with weak topographic slopes in the west-southwest east-northeast direction (according to model topography). Results from s5 at 10 m depth are shown in Fig. 4.16. The temperature is well reproduced by the model. The velocity frequency is described fairly well with a slight over-representation of low velocities. The directional frequency and the transport in different directions are not captured to the degree that is desired. Observations show an unordered velocity direction with a main direction toward east-northeast while the velocity direction is more distinct in the model with a clear west-southwest direction. The model topography is possibly not well represented at this position (i.e., results from the model indicates a clear topographic steering of the currents that is not seen in the observations).

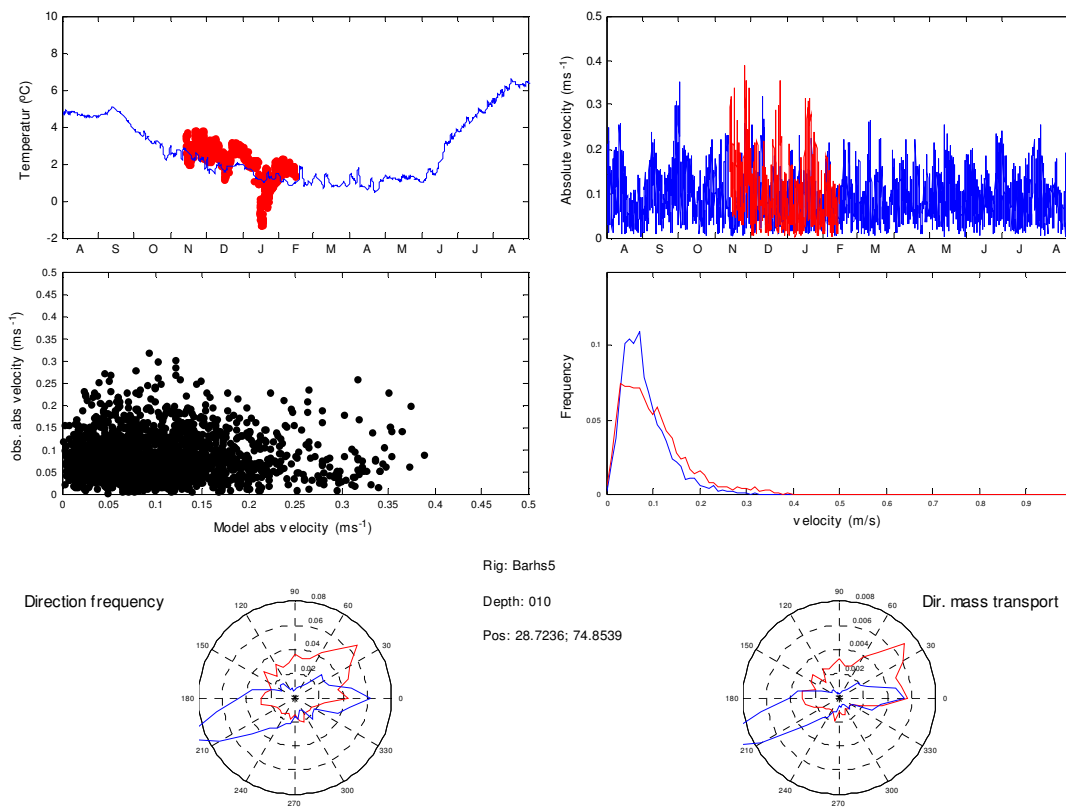


Figure 4.16: Results from current rig Barh_s5.

5 Release of icebergs

One of the purposes with this exercise is to provide a tool for evaluating the distribution of icebergs in the Barents Sea. Accordingly, one test of the model is to examine the long term transport pattern of icebergs from different regions. As stated in the introduction, the main source of icebergs for the Barents Sea is probably Renown Glacier at Franz Josef Land, and we thus release a number (in this study we use 10) of icebergs in different areas around Franz Josef Land. There is no information on the main path of the icebergs and we release icebergs at several locations on the southern, northern, and eastern side of Franz Josef Land. The timing of the iceberg releases may also be an important parameter, again little is known. However, it is likely that the main calving takes place in late summer/early autumn and we therefore release icebergs at the beginning of the available forcing dataset, i.e., Aug. 1, 1987, and run the model for 13 months. Notably, we have made more experiments to verify the general findings of these experiments but have chosen to limit the number of figures.

Svalbard is also a source of icebergs for the Barents Sea and we consider release of icebergs on the northern and eastern side of Svalbard to study the general transport patters for Barents Sea icebergs having Svalbard as their origin.

5.1 Franz Josef Land icebergs

The Renown Glacier is located on the southern side of the largest island in the Franz Josef archipelago. We have tried to release icebergs in the vicinity of the coast; however, the icebergs we use (200 m long and 70 m deep) will become grounded initially and we therefore release the icebergs at some distance from the coast. As a sensitivity study we release icebergs both east and west of the Renown glacier. Furthermore, since the movement of icebergs is slow and many of the icebergs remains in the area southeast of Franz Josef Land for a long time we release icebergs at a southeastern position to study long term movements of the icebergs. The movement of icebergs on the northern side of Franz Josef Land is also considered.

5.1.1 Releases south of Franz Josef Land

When releasing the icebergs south of the Renown Glacier the icebergs start to drift eastward (Fig. 5.1 left panel). Some distance to the east the icebergs start to move southwards and later on westward with the Persey current. In this experiment all of the icebergs reach the Barents Sea within a few months. It takes about 100 days to move to the position south of the release position. The icebergs remain well grouped together for about 120 days; thereafter the different icebergs may take very different paths: notably, the separation of the pathways takes place at a location with weak topographic forcing where the Persey current apparently move over a shallow flat topographic ridge. Some of the icebergs continue westward while others start to move eastward reaching the northern tip of Novaya Zemlya after some time. When reaching this area the icebergs are advected out of the model domain and the iceberg calculation is terminated. Icebergs that move westward reach well into the Barents Sea during spring/summer, and the icebergs start to melt quickly when reaching warm waters in summer (Fig. 5.1 right panel). Looking at the iceberg melt rates the icebergs decay rather slowly during autumn-winter-spring loosing about 40 m in length in this period. The melting was quick at the initial release, continuing at a slower rate thereafter.

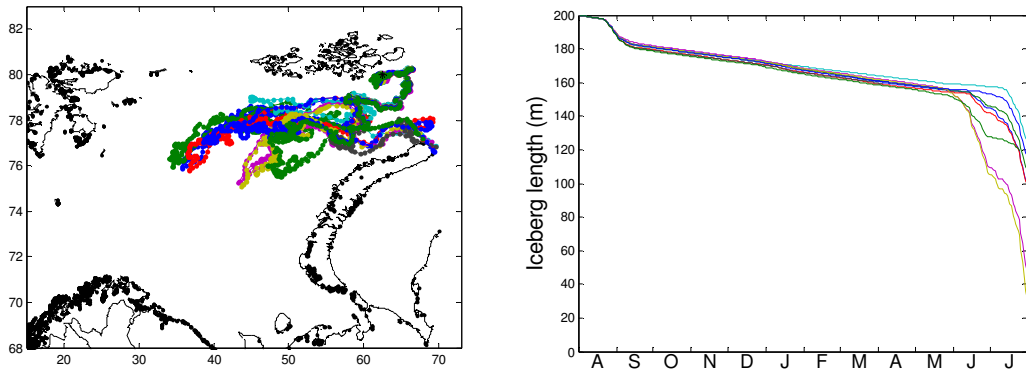


Figure 5.1: Release of icebergs south of the Renown Glacier in Franz Josef Land. Left panel shows the trajectories for thirteen months and the right panel shows the iceberg length.

5.1.2 Releases south-southwest of Franz Josef Land

To further study the main advection path of the icebergs south of Franz Josef Land we released some icebergs on the middle-to-western part. In these experiments there were initially steady movements of icebergs eastward (this can be hard to spot in the uppermost panel of Fig. 5.2 but a closer inspection shows that the icebergs initially move eastward in agreement with the other experiments shown in this section). However, the exact trajectories depend greatly on the release position. We accordingly speculate that the exact date of the release may also be an important parameter.

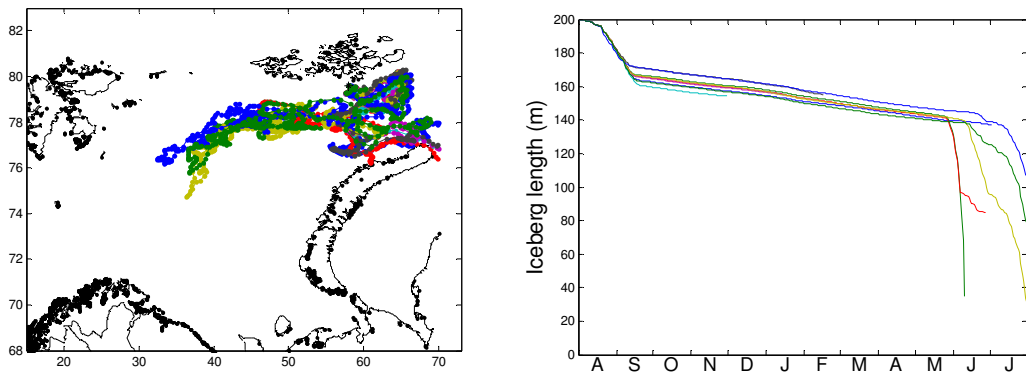


Figure caption on next page

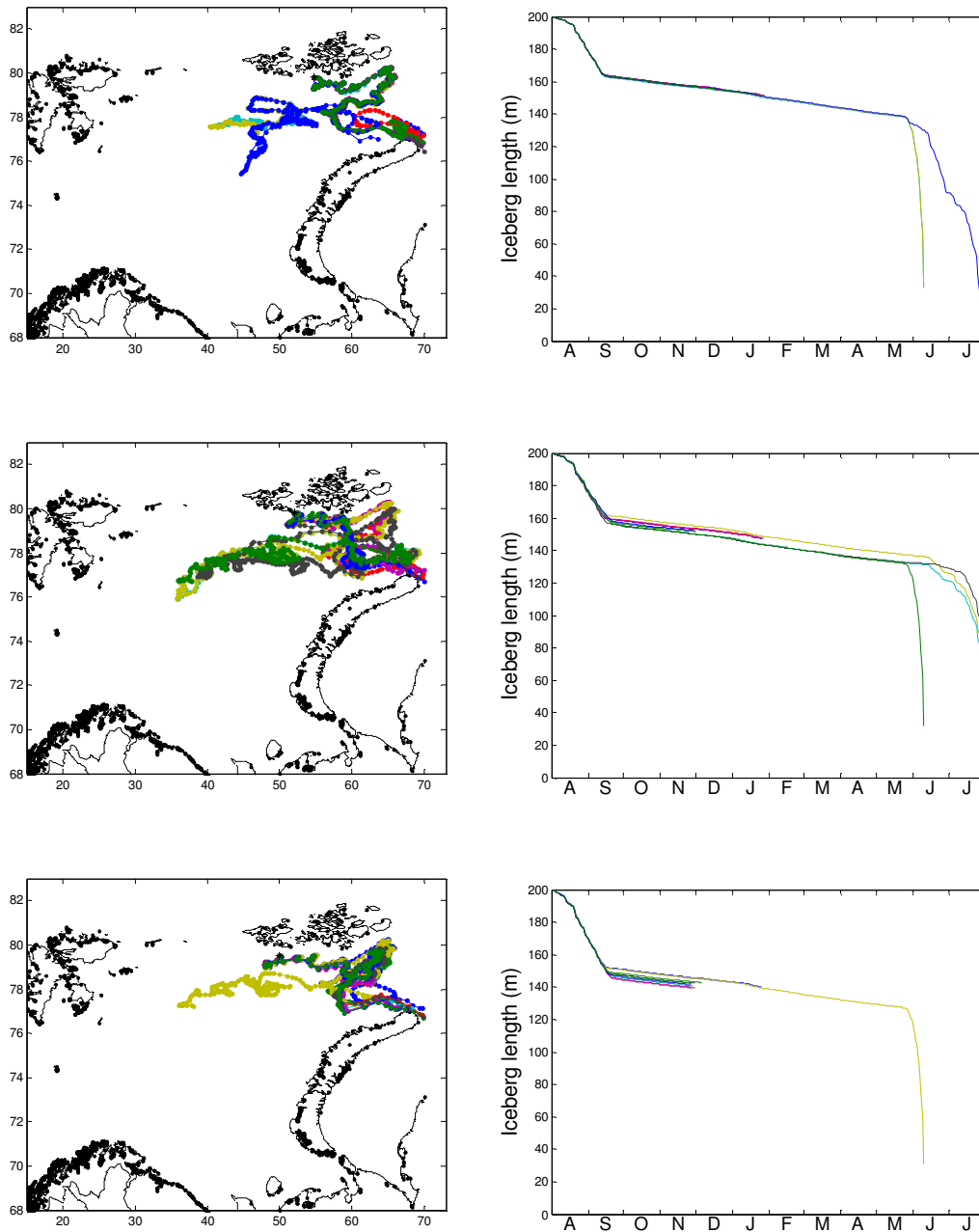


Figure 5.2: Trajectory of icebergs released south south-west of Franz Josef Land; the release position is more westward in lower panels than in upper panels. Left panels show the trajectories for thirteen months and the right panels show the iceberg length.

5.1.3 Releases east of Franz Josef Land

The experiment where we release icebergs in the eastern part of the Franz Josef Land archipelago is shown in Fig. 5.3. The icebergs initially move eastward while turning south after some time. Most of the icebergs move rather slowly and most icebergs (8 of 10) do not move outside the Franz Josef Land region during this calculation. Two of the icebergs move

faster and they take the general advection pathway of the icebergs released south of Franz Josef Land.

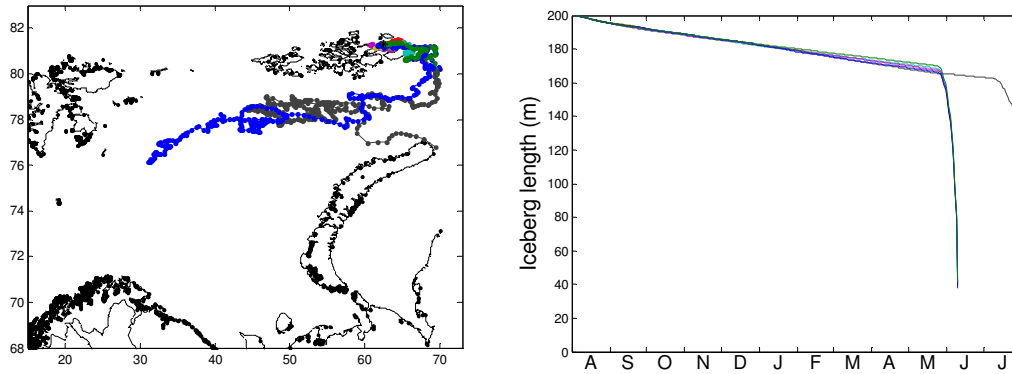


Figure 5.3: Trajectory of icebergs released in the eastern part of Franz Josef Land archipelago. Left panel shows the trajectories for thirteen months and the right panel shows the iceberg length.

5.1.4 Releases southeast of Franz Josef Land

The general pattern is that the icebergs move eastward on the southern border of the Franz Josef Land. When reaching a region somewhat east of the archipelago the icebergs move southward for some time before starting to move westwards. To see if this is a stable feature, and also to check the trajectories in the following year of icebergs that get stuck in this region, we start an experiment using the positions of the southeastward branch of the general advection pathway. The result is displayed in Fig. 5.4. The result is in agreement with the overall trajectory analysis for icebergs released south of Franz Josef Land. The icebergs move southward for some time and start to move westward at about 67E. The westward movements continue for some time until the icebergs reach a point where the trajectory bifurcates into one branch eastward to the northern tip of Novaya Zemlya, and the other branch into the Barents Sea.

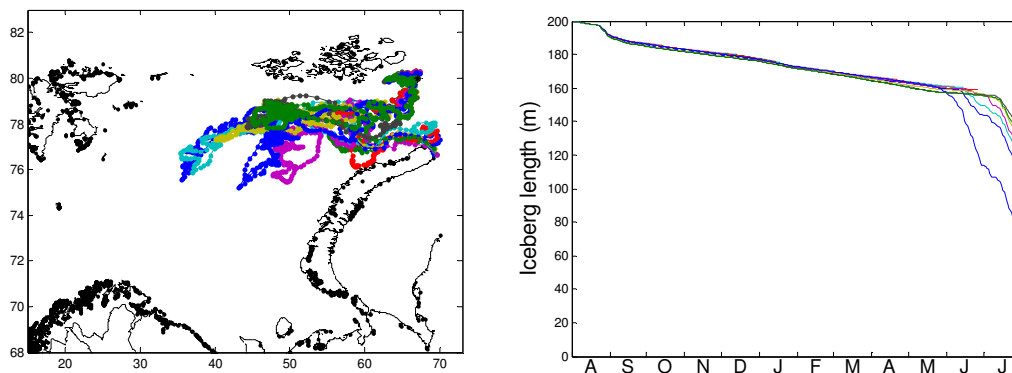


Figure 5.4: Trajectory of icebergs released southeast of Franz Josef Land. Left panel shows the trajectories for thirteen months and the right panel shows the iceberg length.

5.1.5 Releases north of Franz Josef Land

All icebergs released north of Franz Josef Land travel westward and southward: the icebergs' movements are relatively slow (possible due to grounding) and the experiment shows that most icebergs will survive for more than one year. However, two of the icebergs take a more northern path, which appears to be quicker, and these icebergs end up between Franz Josef Land and Svalbard about 8-10 months after the release (Fig. 5.5). Three of the icebergs seem to take trajectories through the Franz Josef Land archipelago, though the trajectories stop before the full passage is made.

The length of the icebergs decreases slowly in the northern areas and reaches a length of 150 m after 1 year. However, two of the icebergs move further to the south and melt somewhat quicker. One of the icebergs actually moves into quite warm water and would probably melt altogether in another month or so.

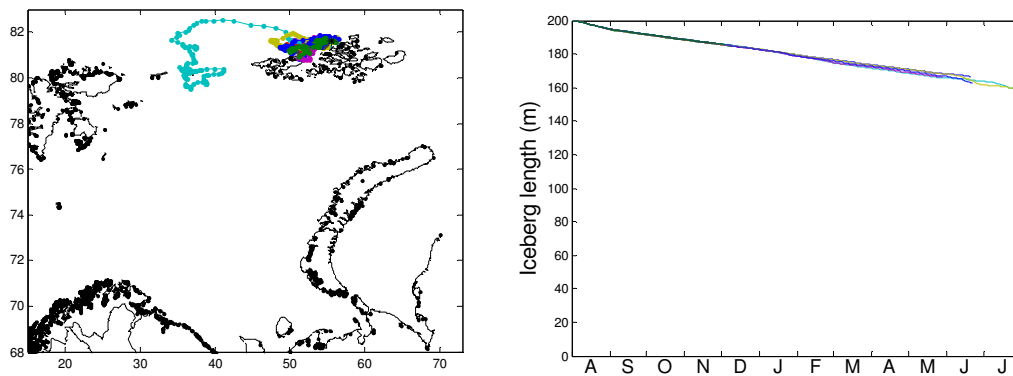


Figure 5.5: Trajectory of icebergs released northern shore of Franz Josef Land. Left panel shows the trajectories for thirteen months and the right panel shows the iceberg length.

As noted above, many of the icebergs remain north of Franz Josef Land the entire model year. Accordingly, we consider two experiments using starting points characteristic for the end position of the eastern icebergs (Fig. 5.5). The results of the experiment are displayed in Fig. 5.6. Most of the icebergs at these released positions travel west and southwards toward the Barents Sea. However, for the easternmost of the two positions, one iceberg moves towards Franz Josef Land while three icebergs end up north of Svalbard. All icebergs moving east and southwards remain large until the middle of June when they melt very quickly.

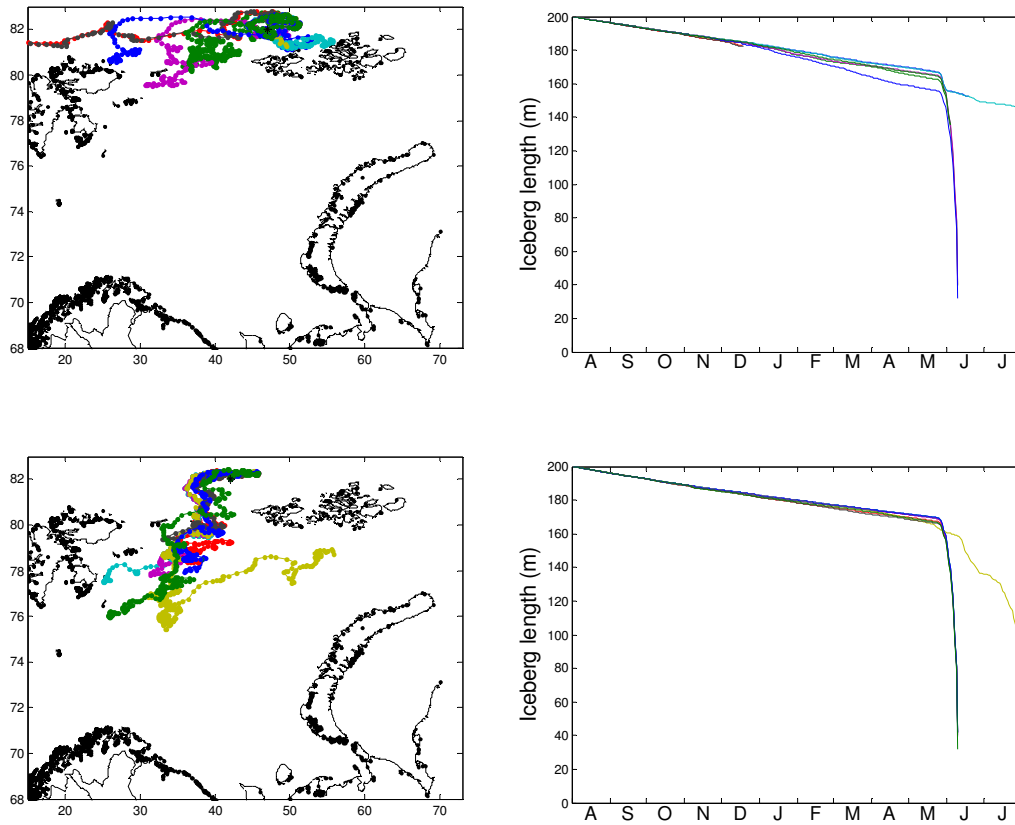


Figure 5.6: Trajectory of icebergs released northwest of Franz Josef Land. Left panels show the trajectories for thirteen months and the right panels show the iceberg length.

5.2 Releases in Svalbard area

To investigate the modeled iceberg movements in the Svalbard area we release icebergs north of Svalbard, and at two positions east of Svalbard. From the position north of Svalbard most icebergs move very slow, possible due to groundings. The movement is generally eastward toward the Barents Sea. However, the slowness of the movement implies that they do not reach the Barents Sea before being melted in the summer of 1988 (the area north of Svalbard is generally quite warm due to the NwAC (Fig. 3.1 and Fig. 3.2)). From positions east of Svalbard the general pathway is eastward into the Barents Sea. When reaching the northern side of the Hopen trench the general advection is southwestward following the shallow area on the Spitsbergen Bank. This is in agreement with the advection pathways (and iceberg sightings) observed during IDAP (Spring, 1994). The water is relatively cold all year on the northern part of the Spitsbergen Bank while summer temperatures are quite high on the southern areas close to the Hopen trench. Accordingly, icebergs reaching southern positions will melt rapidly (Fig. 5.5 lower right panel).

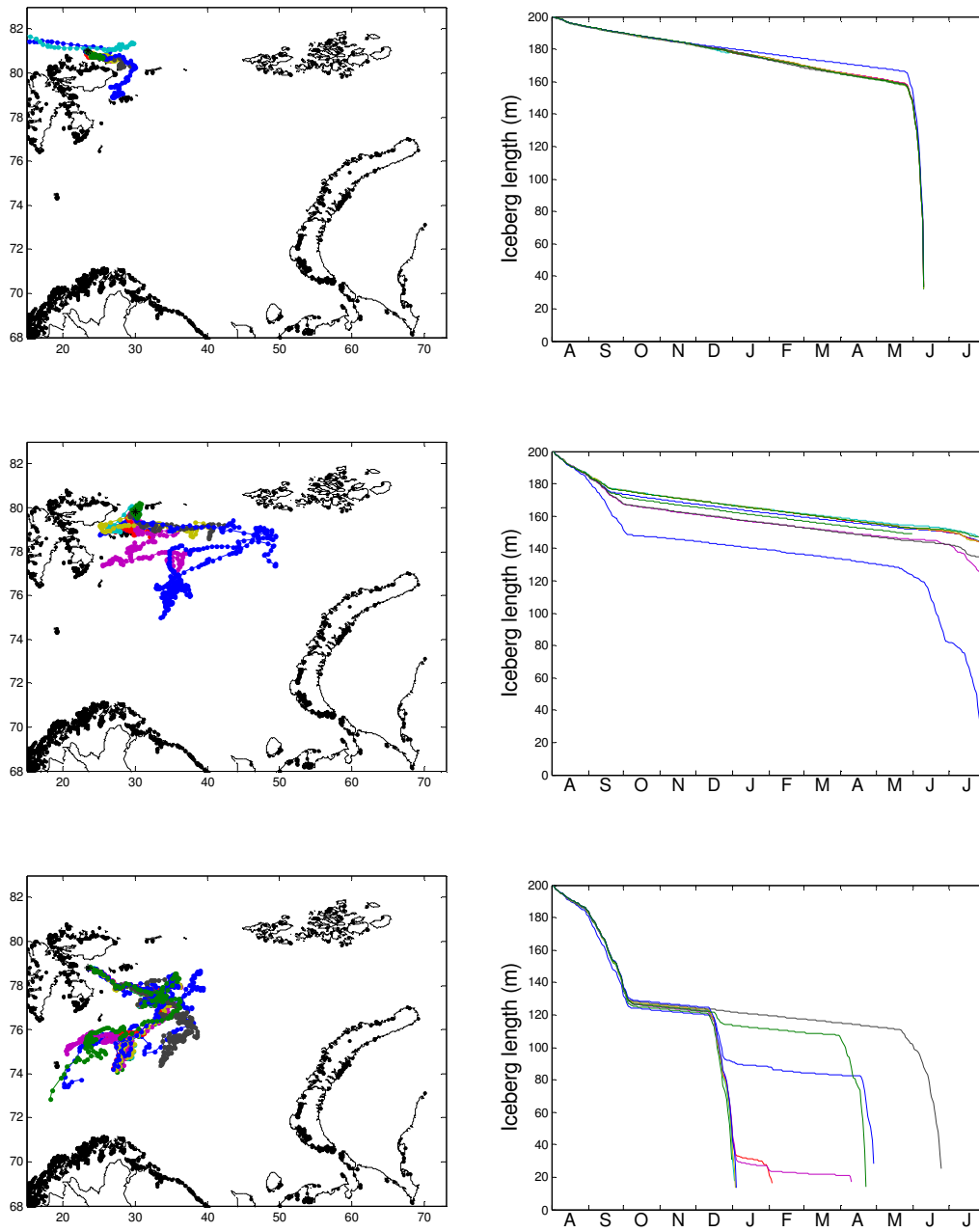


Figure 5.7: Trajectory of icebergs released north and east of Svalbard. Left panels show the trajectories for thirteen months and the right panels show the iceberg length.

6 Results and discussion

In this study we validate ocean current results from a hindcast study that will provide forcing data for an iceberg model. The hindcast study results will mainly be used for

- Validation study of iceberg trajectories during 1987 and 1988 (Broström *et al.*, 2009).
- Studies of iceberg advection pathways and iceberg climatology for the Barents Sea to be carried out by StatoilHydro.

More detailed summaries for the validation using IDAP mooring data (Spring, 1994), and the validation from studying general advection pathways for icebergs are outlined below.

6.1 Summary for validation from IDAP moorings

The main results from the comparison of model data with mooring observations are:

1. Temperature:
 - a. Temperature is modeled with fair accuracy. However, the model may be slightly too warm at cold temperatures both in winter and summer. This may have consequences for the melting rates of the icebergs in long model runs.
 - b. Observations for temperature generally show greater variability than model results.
2. Currents:
 - a. The spectral distribution of the velocity strength agrees well with observations.
 - b. Spectral distribution of current direction agrees well with observations.
 - c. Transport in different directions is well modeled in strength and direction.
 - d. The correlations between modeled and observed currents are weak.
 - e. Model agreement with observation increases if a time lag between model and observations is introduced: however, even after this “correction” the model results remains poorer than the quality we desire.
 - f. Observations show a very clear peak in the power spectral density at the M2 tide and the inertial frequency: however, the power spectral frequency distribution for velocity from the model is wider than from observations. The reason for this is unknown.

6.2 Summary for iceberg movements

In this study we have investigated the movements of icebergs released from the major sources of icebergs in the Barents Sea area. We found an anti-clockwise (cyclonic) circulation around the Franz Josef Land such that icebergs released on the northern shore move westward while icebergs released on the southern shores move mainly eastward. The eastward movement

south of Franz Josef Land is very stable in the experiments, continuing until the icebergs reach a deep trench. Here the icebergs start to move southwards. The southward movement continues following the topography and thus become eastward at some distance to the south. The iceberg groups generally remain clustered until reaching the shallow area south of Franz Josef Land.

We speculate that there exist preferred advection pathway of icebergs from both Franz Josef Land and Svalbard toward the northern Barents Sea. However, there is a great scatter in the advection pathways and additional studies are called for if this issue is to be resolved. The release time of the icebergs may also be an important variable to consider. Longer time series are also needed for more accurate evaluation of the pathways of icebergs in different climate forcing.

6.3 Final comments

The main result of this study is that the model reproduces statistical features of the IDAP mooring observations and we conclude that the model should be able to reproduce the main features of iceberg movements and icebergs melting rates in the analyzed area. We also find that the model does not give very precise predictions on the current at specific times, judging from the poor correlation between model and observations in a scatter-scatter plot. The reason for this remains somewhat unknown but it may be that the model does not reproduce tidal motions in the correct way, as suggested by the differences in the frequency power spectrum (Fig. 4.11). However, more detailed studies may be needed for more accurate statement of this discrepancy between model and observations.

The advection pathways of icebergs are more difficult to judge as there are few observations of such pathways over long time. We find that the advection pathways are largely controlled by topography. However, further studies may be needed to confirm these findings and to evaluate if observations support this statement. One possible test for a future study may be to investigate how well iceberg trajectories follow topographic features and compare (statistical) model results with observations. This would be a test of the dynamical features of the model rather than describing the exact trajectory correctly in space and time. Nevertheless, our aim is to determine the trajectories of icebergs, which constitute time integral of velocity. So, even though there are problems with the temporal correlations between model results and observations, the positive results from the velocity statistics make up for this deficiency, at least to some extent.

Finally it should be noted that the analysis only covers one year and this may represent an uncertainty: it is recommended that a longer forcing dataset is used for more reliable estimates on iceberg dynamics in the Barents Sea area. However, the main purpose of the present study was to validate an operational system for iceberg drift, not to investigate the inter-annual variability of iceberg pathways or other aspects of iceberg drift of time scales longer than one year.

Acknowledgement

Kenneth Johannessen at StatoilHydro provided the data from the IDAP study. Furthermore, he gave very valuable comments on an earl version of this report.

References

- Abramov, V.A., 1992: Russian iceberg observations in the Barents Sea 1933-1990. *Polar Research* 11, 93-97.
- Albretsen, J. & I. Burud, 2006: Assimilation of sea surface temperature and sea ice concentration in a coupled sea ice and ocean model. In: H. Dahlin, N.C. Flemming, P. Marchand and S.E. Petersson (Editors), *European Operational Oceanography: Present and Future*. 4th International Conference on EuroGOOS, Brest, France, pp. 663-668.
- Blumberg, A.F. & G.L. Mellor, 1987: A description of a three-dimensional coastal ocean circulation model. In: N.S. Heaps (Editor), *Three-Dimensional Coastal Ocean Models*. AGU Coastal and Estuarine Series, American Geophysical Union, Washington D.C.
- Broström, G. & K. Christensen, 2008: Waves in ice. Research report, 5, Norwegian Meteorological Institute, Oslo, Norway. pp. 68.
- Broström, G., A. Melsom, M. Sayed & I. Kubat, 2009: Iceberg modelling at met.no: description and validation of iceberg model. Report series, 17, Norwegian Meteorological Institute, Oslo, Norway. pp. 36.
- Cavalieri, L., *et al.*, 2007: Wave modelling - The state of the art. *Progress in Oceanography* 75, 603-674.
- Engedahl, H., 1995: Implementation of the Princeton Ocean Model (POM/ECOM3D) at the Norwegian Meteorological Institute. Research Report, 5, Norwegian Meteorological Institute, Oslo, Norway.
- Flather, R.A., 1981: Results from a model of the north-east Atlantic relating to the Norwegian coastal current. In: R. Sætre and M. Mork (Editors), *The Norwegian Coastal Current: Vol II*. University of Bergen, Bergen, Norway, pp. 427-458.
- Furevik, T., 2001: Annual and interannual variability of Atlantic water temperatures in the Norwegian and Barents Seas: 1980-1996. *Deep-Sea Research* 48, 383-404.
- Gjevik, B., E. Nost, & T. Straume, T, 1990: Atlas of tides on the shelves of the Norwegian and the Barents Sea, Department of Mathematics, University of Oslo, Oslo, Norway.
- Hagen, J.O., J. Kohler, K. Meldvold & J.G. Winther, 2003: Glaciers in Svalbard: mass balance, runoff and freshwater flux. *Polar Research* 22, 145-159.
- Hibler, W.D., III, 1979: A dynamic thermodynamic sea ice model. *Journal of Physical Oceanography* 9, 815-846.
- Ingvaldsen, R.B., 2005: Width of the North Cape Current and location of the Polar Front in the western Barents Sea. *Geophysical Research Letters* 32, L16603, doi:10.1029/2005GL023440.
- Ingvaldsen, R.B., L. Asplin & H. Loeng, 2004: Velocity field of the western entrance to the Barents Sea. *Journal of Geophysical Research* 109, C03021, doi:10.1029/2003JC001811.
- Keghouche, I., L. Bertino & S. Sandven, 2007: Iceberg modeling in the Barents Sea part I: Initial tests. Technical Report, Mohn Sverdrup Department, Nansen Environmental and Remote Sensing Centre. pp. 11.
- Komen, G.J., L. Cavaleri, M. Donelan, K. Hasselmann, S. Hasselmann and coauthors, 1994:

- Dynamics and modelling of ocean waves. Cambridge University Press, Cambridge, 532 pp.
- Kubat, I., M. Sayed, S.B. Savage, T. Carrieres & G. Crocker, 2007: An operational iceberg deterioration model, 17'th International Offshore and Polar Engineering Conference.
- Kubat, I., M. Sayed, S.B. Savage & T. Carriers, 2005: An operational model of iceberg drift. *International Journal of Offshore and Polar Engineering* 15, 125-131.
- Kwok, R., W. Maslowski & S.W. Laxon, 2005: On large outflows of Arctic sea ice into the Barents Sea. *Geophysical Research Letters* 32, L22503, doi:10.1029/2005GL024485.
- LaCasce, J.H., 2000: Float and f/H. *Journal of Marine Research* 58, 61-95.
- Lichey, C. & H.H. Hellmer, 2001: Modeling giant-iceberg drift under the influence of sea ice in the Weddell Sea, Antarctica. *Journal of Glaciology* 47, 452-460.
- Liestøl, O., 1969: Glacier surges in west Spitsbergen. *Canadian Journal of Earth Science* 6, 895-897.
- Liestøl, O., 1973: Glaciological work in 1971. *Norwegian Polar Institute Yearbook 1971*.
- Løset, S. & T. Carstens, 1996: Sea ice and iceberg observations in the western Barents Sea in 1987. *Cold Regions Science and Technology* 24, 323-340.
- Mellor, G.L. & T. Yamada, 1982: Development of turbulence closure model for geophysical fluid problems. *Rev. Geophys. Space Phys.* 20, 851-875.
- Nøst, O.A. & P.E. Isachsen, 2003: The large-scale time-mean ocean circulation in the Nordic Seas and Arctic Ocean estimated from simplified dynamics. *Journal of Marine Research* 61, 175-210.
- Røed, L.P. & J. Debernard, 2004: Description of an integrated flux and sea-ice model suitable for coupling to an ocean and atmosphere model. *Research Report, 4, Norwegian Meteorological Institute, Oslo, Norway.* pp. 51.
- Savage, S.B., 2007: Modelling wave radiation stress in the CIS iceberg drift and deterioration program. report to Canadian Hydraulic Centre.
- Schauera, U., H. Loeng, B. Rudels, V.K. Ozhigine & W. Dieckf, 2002: Atlantic water flow through the Barents and Kara Seas. *Deep-Sea Research* 49, 2281–2298.
- Schytt, V., 1969: Some comments on glacier surges in eastern Svalbard. *Canadian Journal of Earth Science* 6, 867-873.
- Skagseth, Ø., 2008: Recirculation of Atlantic Water in the western Barents Sea. *Geophysical Research Letters* 35, L11606, doi:10.1029/2008GL033785.
- Spring, W., 1994: Ice data acquisition program (IDAP) summary report. Dallas E&P Engineering: Dallas. pp. 90.
- Squire, V.A., 2007: Of ocean waves and sea-ice revisited. *Cold Regions Science and technology* 49, 110-133.
- Squire, V.A., J.P. Dugan, P. Wadhams, P.J. Rottier & A.K. Liu, 1995: Of ocean waves and sea-ice. *Annual Review of Fluid Mechanics* 27, 115-168.
- Undén, P., L. Rontu, H. Järvinen, P. Lynch, J. Calvo and coauthors, 2002: HIRLAM-5 Scientific Documentation. Swedish Meteorological and Hydrological Institute,

Norrköping, Sweden.

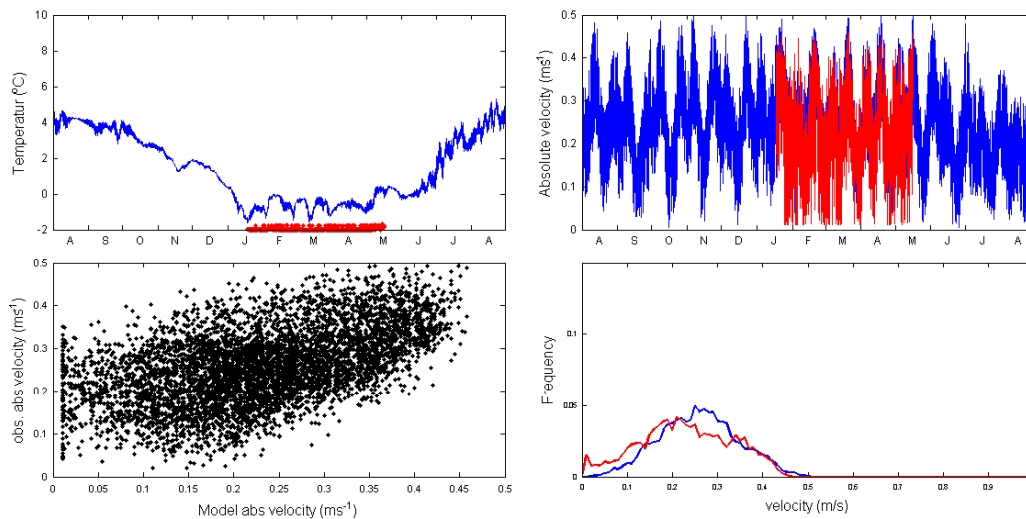
Walin, G., 1972: On the hydrographic response to transient meteorological disturbances. *Tellus* 24, 1-18.

Zubakin, G.K., A.K. Naumov & I.V. Buzin, 2004: Estimates of ice and iceberg spreading in the Barents Sea, 14th International Offshore and Polar Engineering Conference, Toulon, France, pp. 863-870.

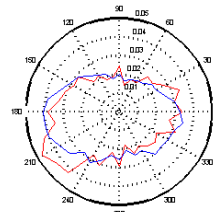
Zubakin, G.K., A.G. Shelomentsev, D.K. Onshuus, L.I. Eide & I.V. Buzin, 2005: Spatial distribution of icebergs in the Barents Sea based on archived data and observations of 2003, 18th International Conference on Port and Ocean Engineering (POAC-2005). "Arctic-Shelf" Laboratory, Arctic and Antarctic Research Institute, St. Petersburg, Russia, Potsdam, USA, pp. 575-583.

Appendix

This appendix describes a detailed model data comparison for current mooring taken during the ISAP program. Each figure covers the period 1 Aug, 1987, to 31 Aug 1988. Each figure contains information on the rig, depth, and position.



Direction frequency

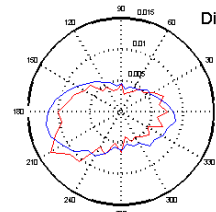


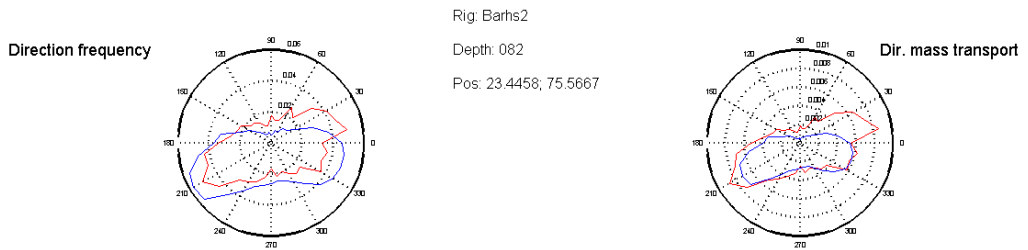
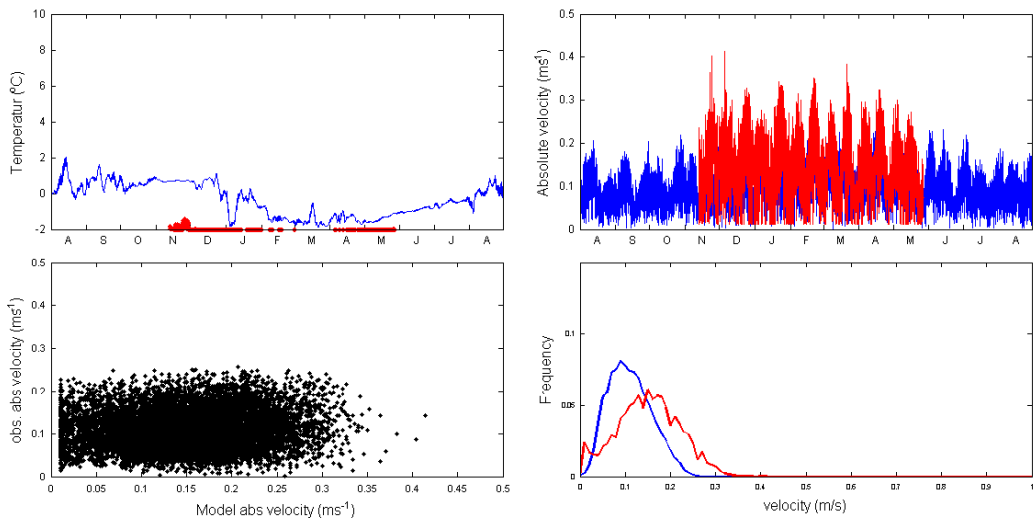
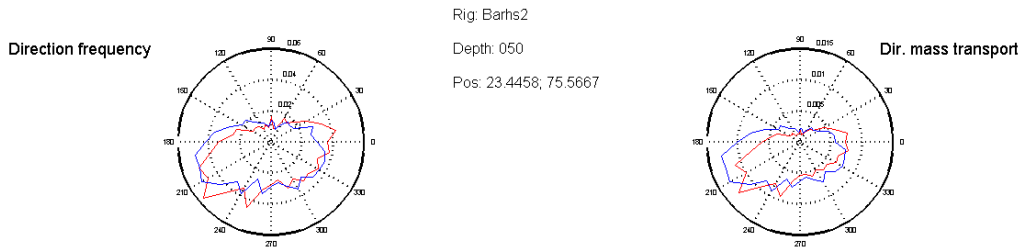
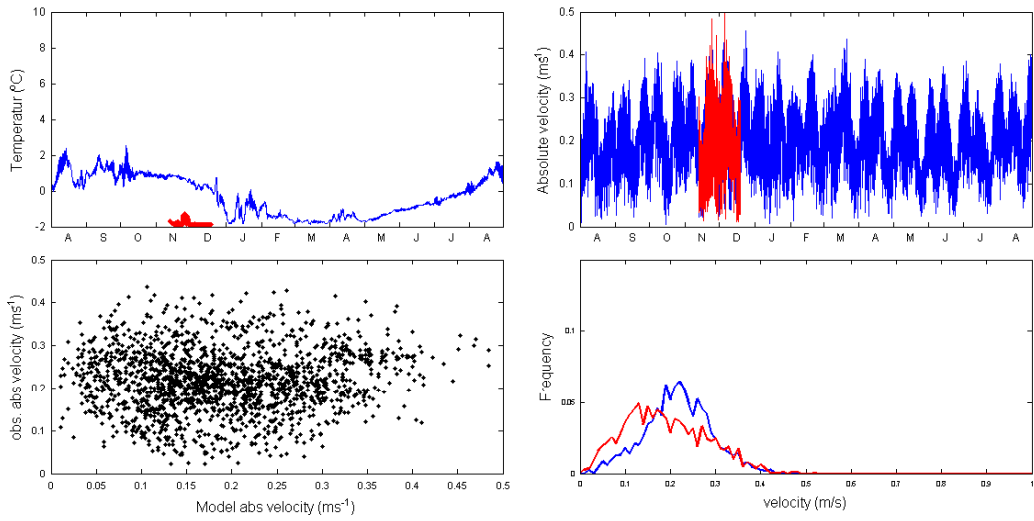
Rig: Barhs1

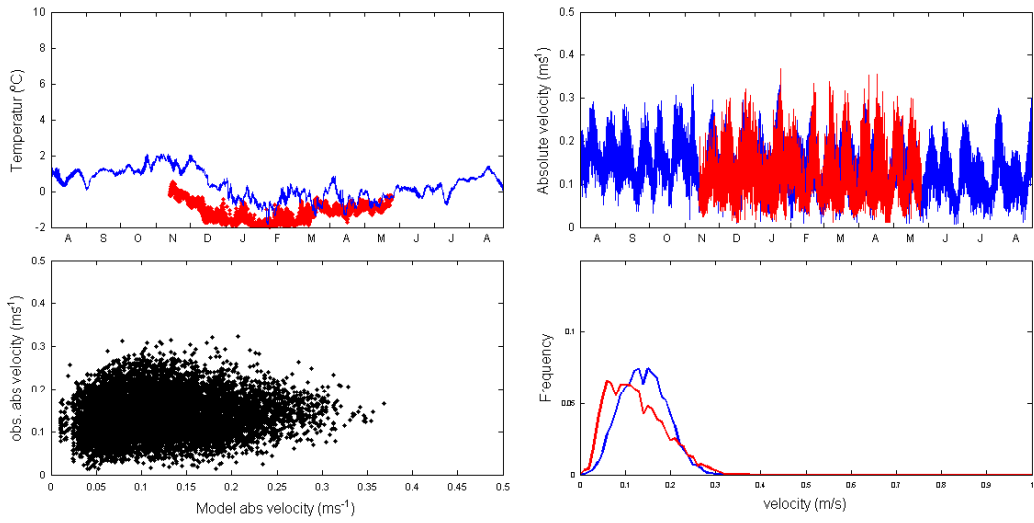
Depth: 063

Pos: 21.2547; 75.0069

Dir. mass transport





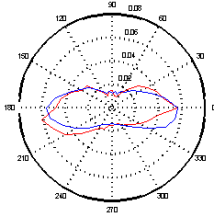


Rig: Barhs3

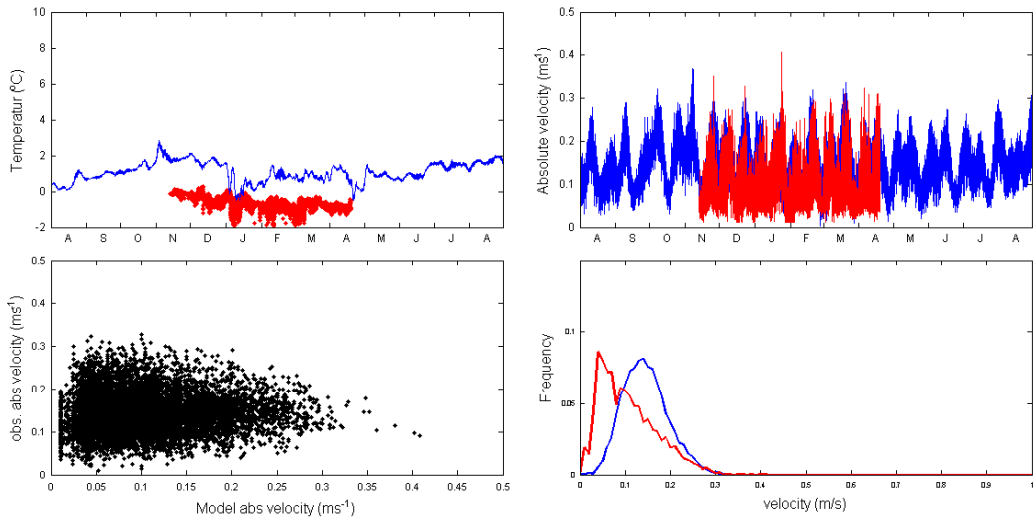
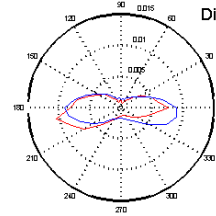
Depth: 050

Pos: 24.9967; 75.3350

Direction frequency



Dir. mass transport

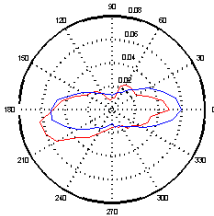


Rig: Barhs3

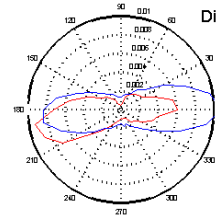
Depth: 100

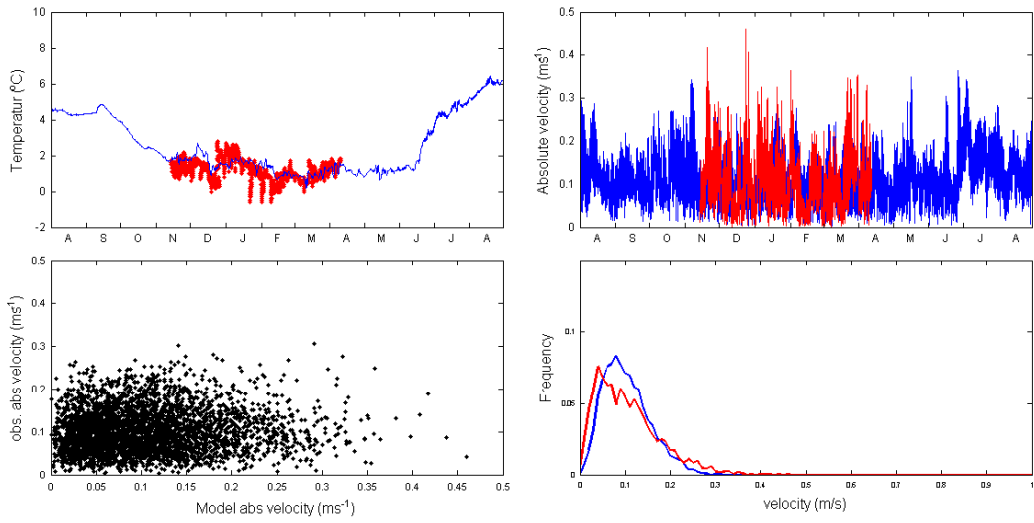
Pos: 24.9967; 75.3350

Direction frequency



Dir. mass transport



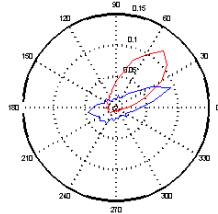


Rig: Barhs4

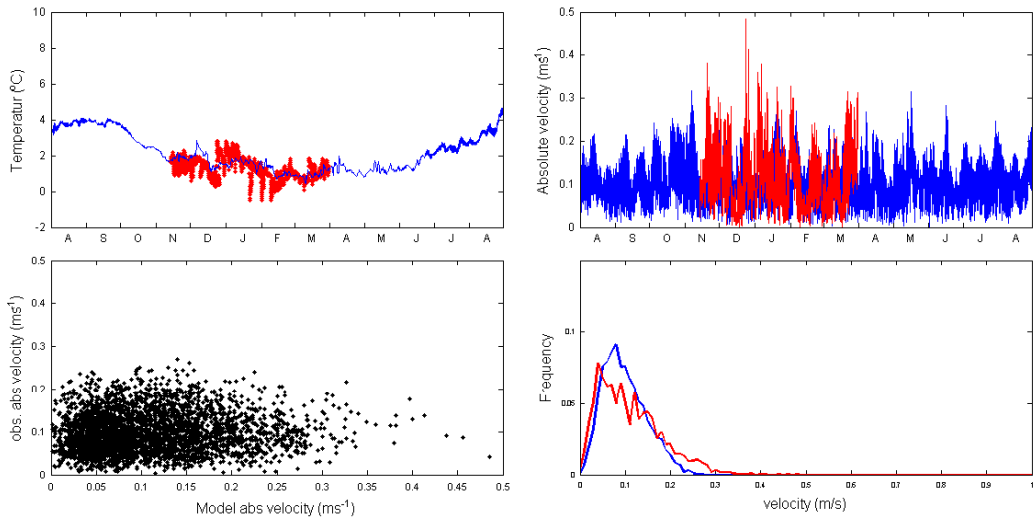
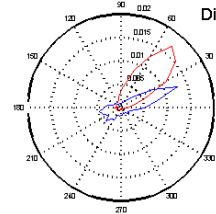
Depth: 010

Pos: 27.1256; 75.0411

Direction frequency



Dir. mass transport

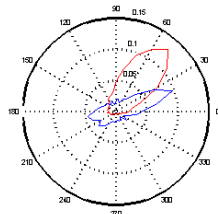


Rig: Barhs4

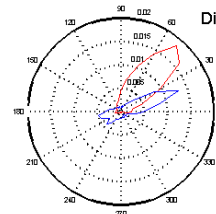
Depth: 025

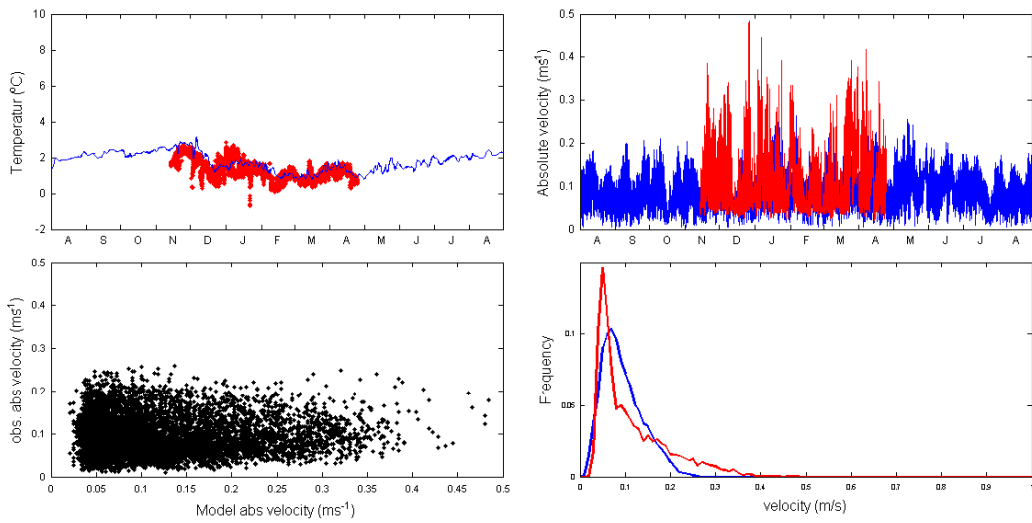
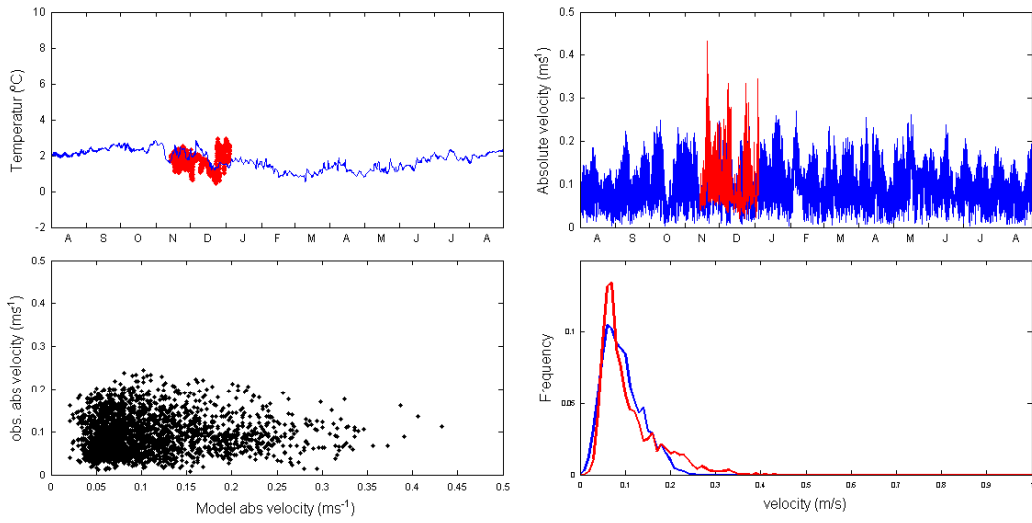
Pos: 27.1256; 75.0411

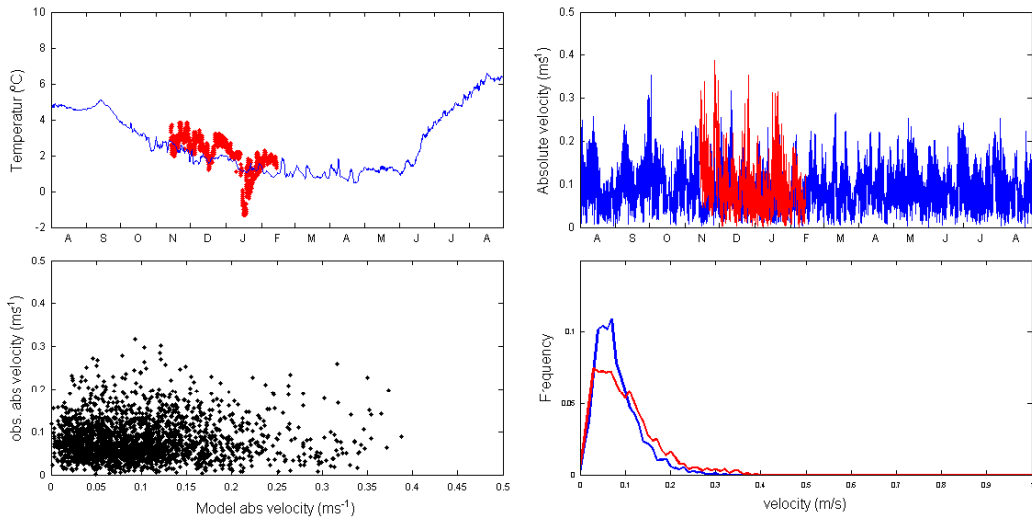
Direction frequency



Dir. mass transport





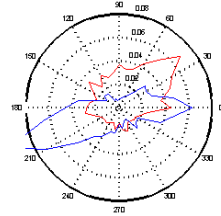


Rig: Barhs5

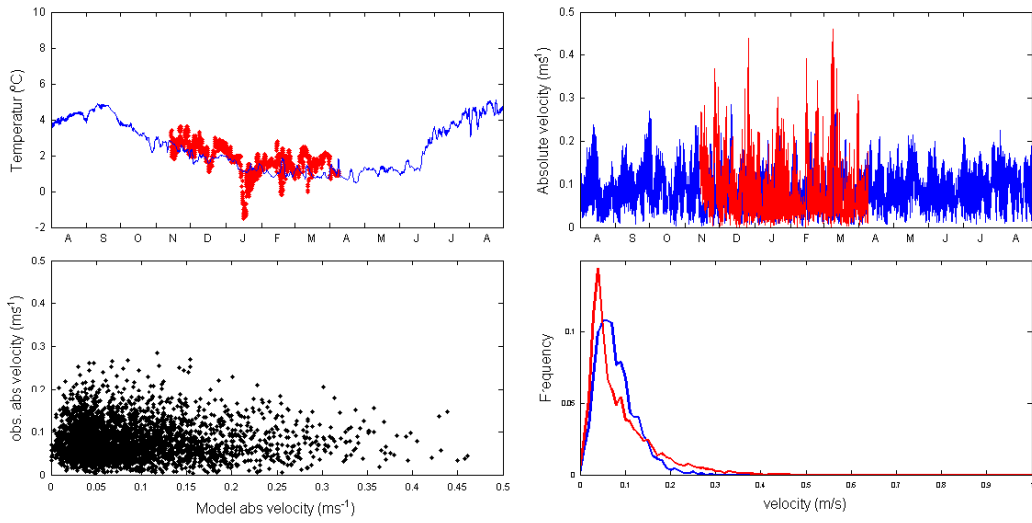
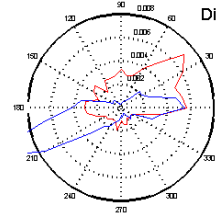
Depth: 010

Pos: 28.7236; 74.8539

Direction frequency



Dir. mass transport

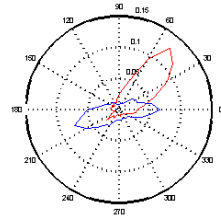


Rig: Barhs5

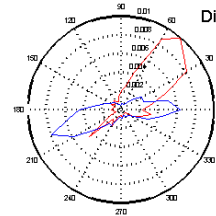
Depth: 025

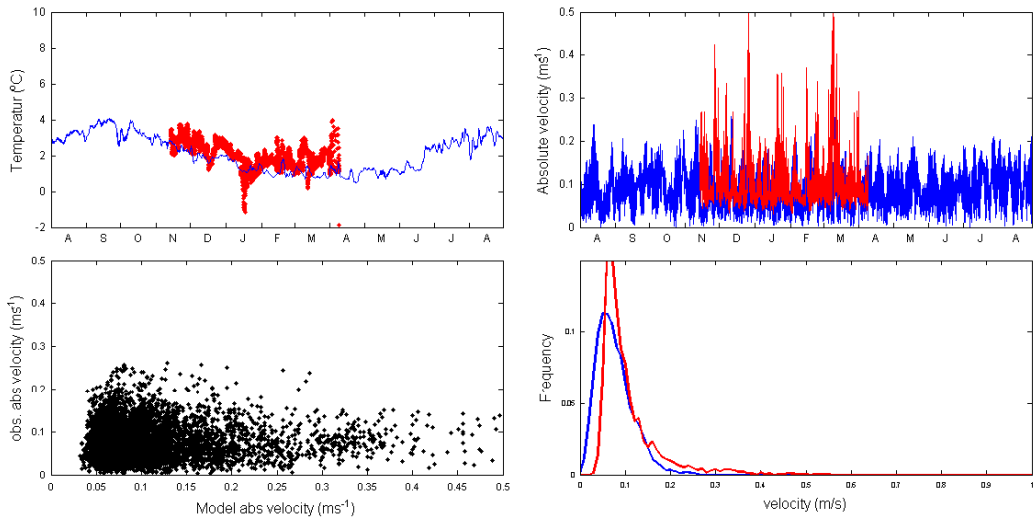
Pos: 28.7236; 74.8539

Direction frequency



Dir. mass transport



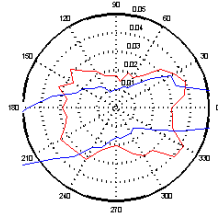


Rig: Barhs5

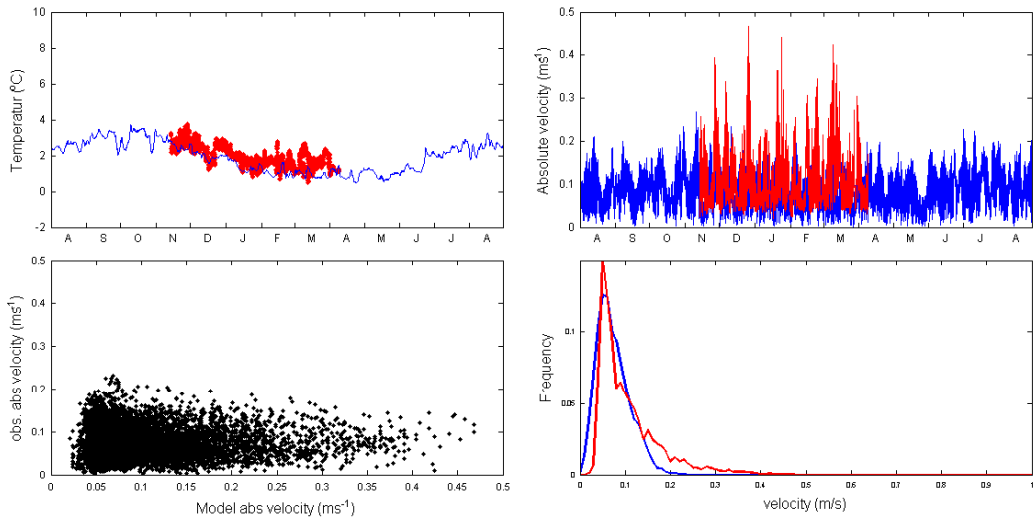
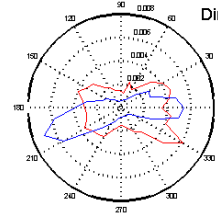
Depth: 050

Pos: 28.7236; 74.8539

Direction frequency



Dir. mass transport

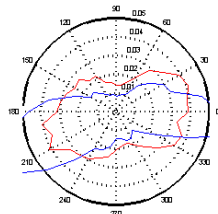


Rig: Barhs5

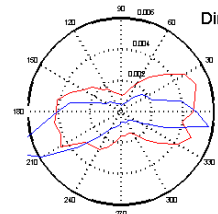
Depth: 100

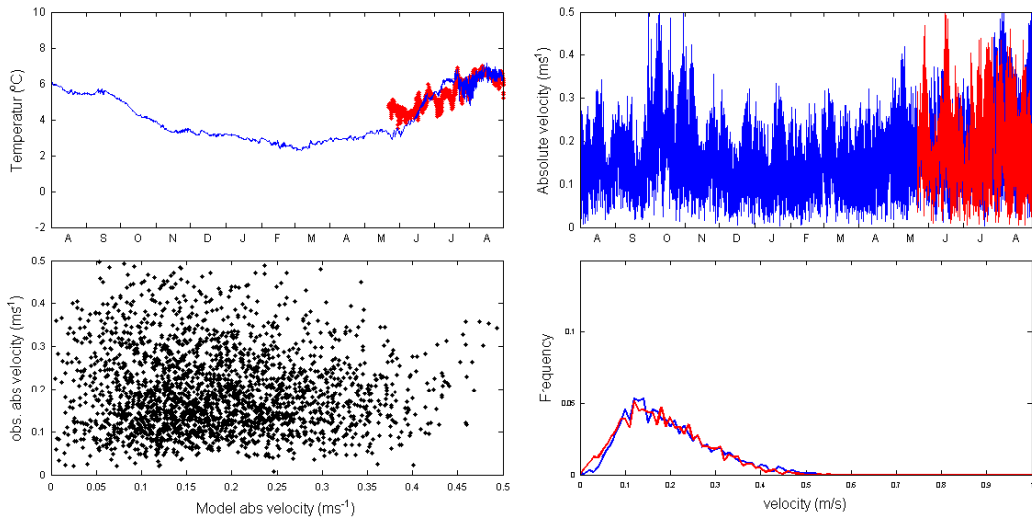
Pos: 28.7236; 74.8539

Direction frequency



Dir. mass transport



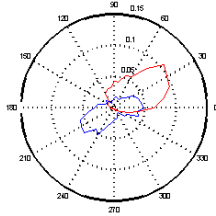


Rig: Barhsa

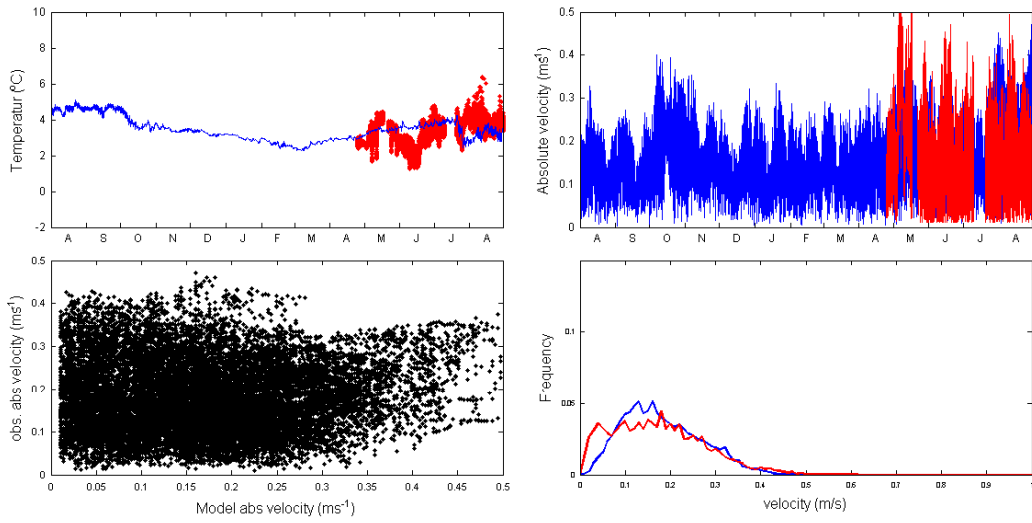
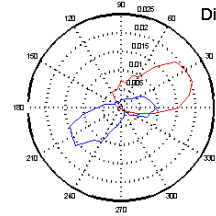
Depth: 010

Pos: 19.9497; 73.8208

Direction frequency



Dir. mass transport

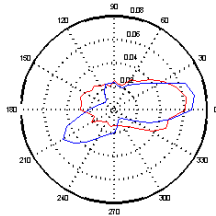


Rig: Barhsa

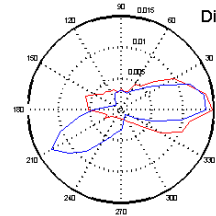
Depth: 050

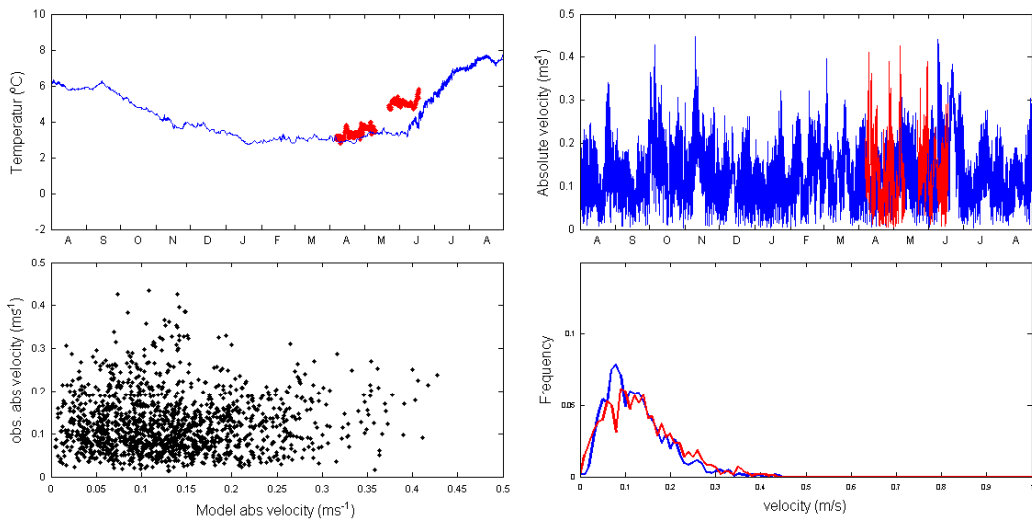
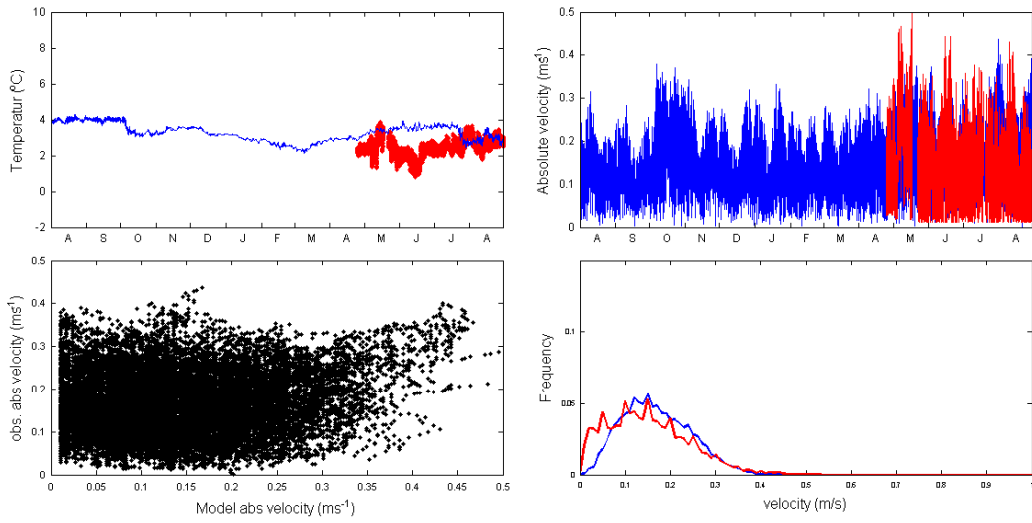
Pos: 20.0167; 73.8389

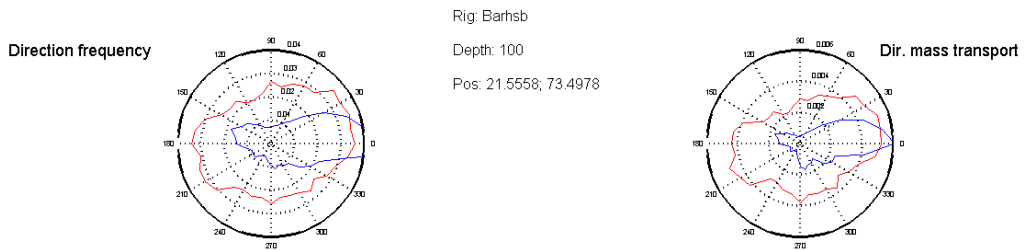
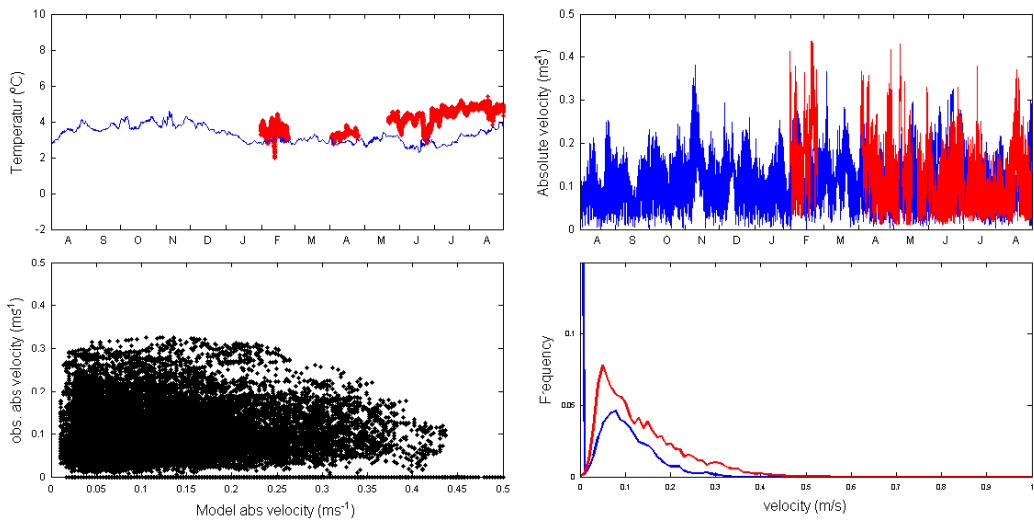
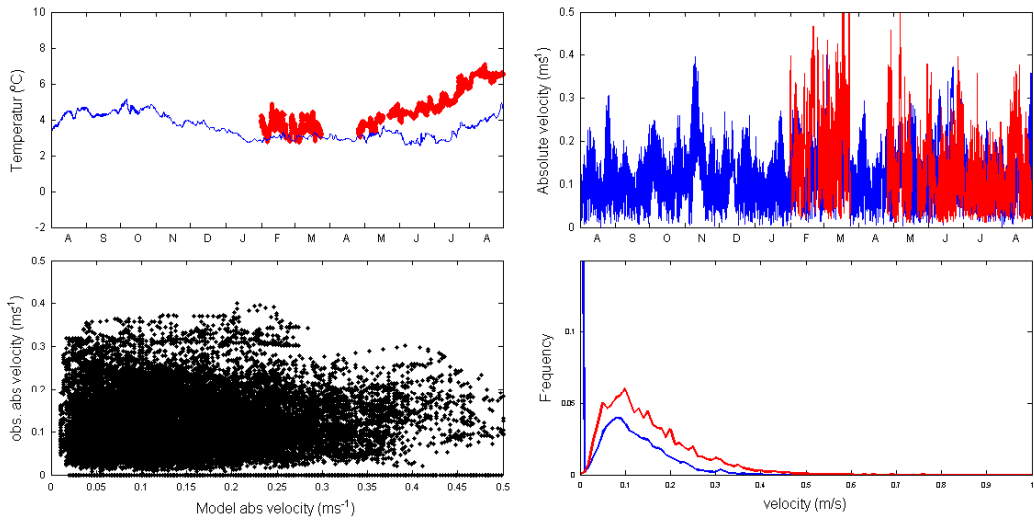
Direction frequency

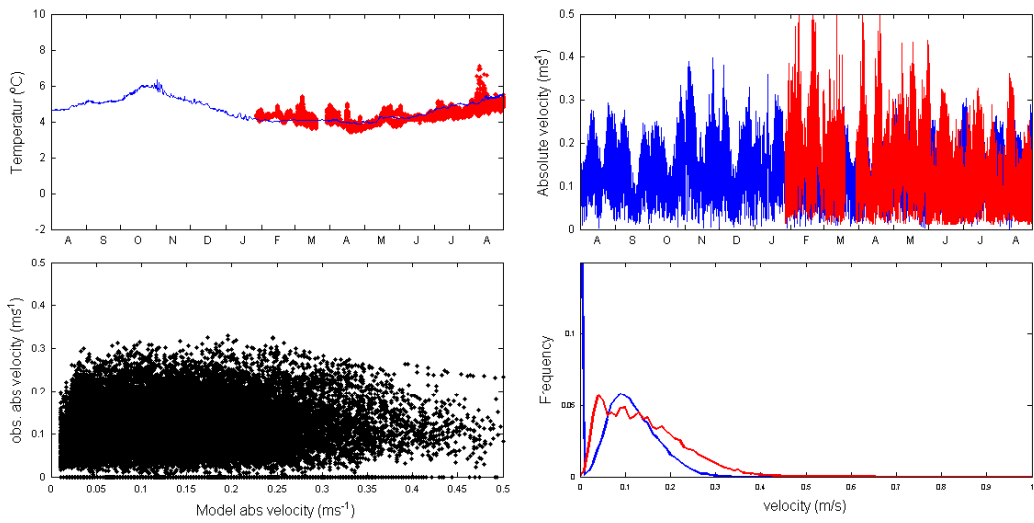
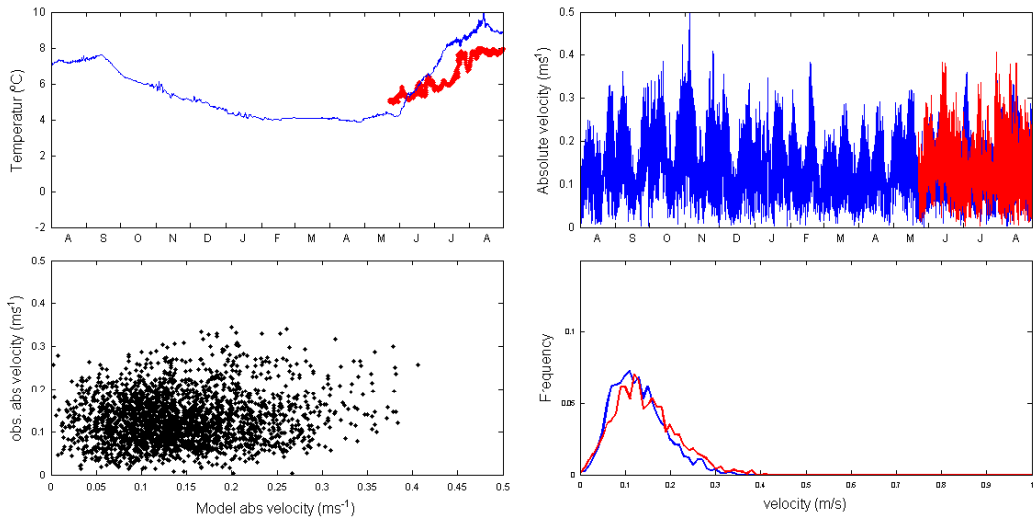


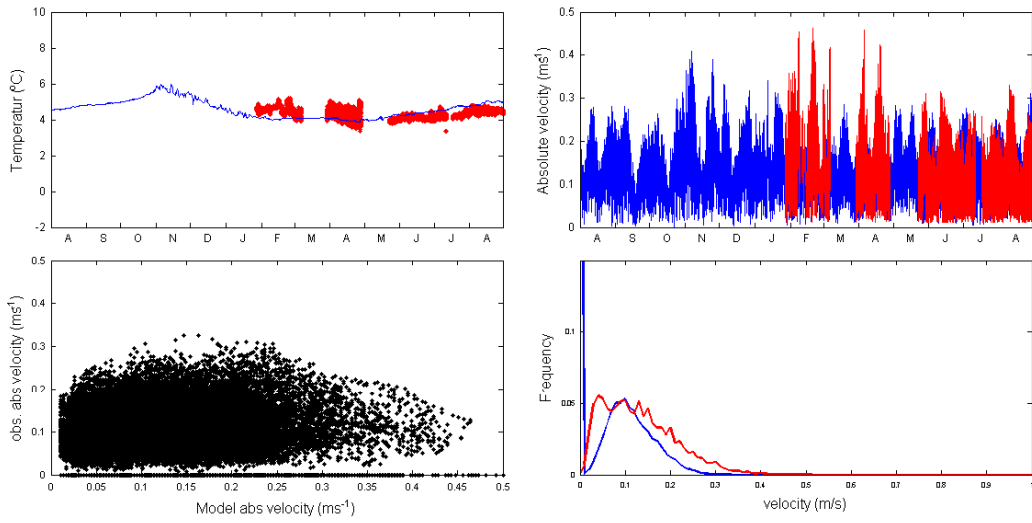
Dir. mass transport









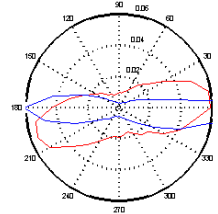


Rig: Barhsc

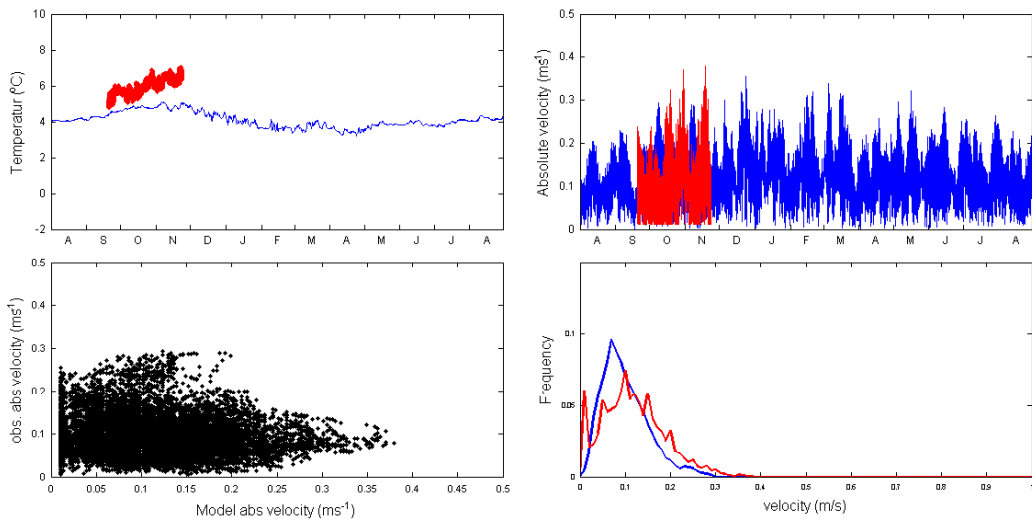
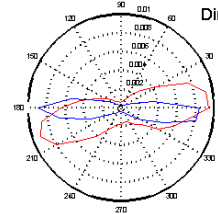
Depth: 100

Pos: 24.3281; 72.3419

Direction frequency



Dir. mass transport

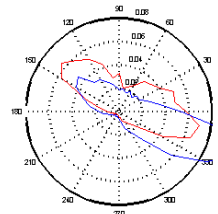


Rig: Barh5

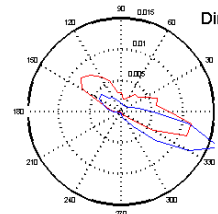
Depth: 100

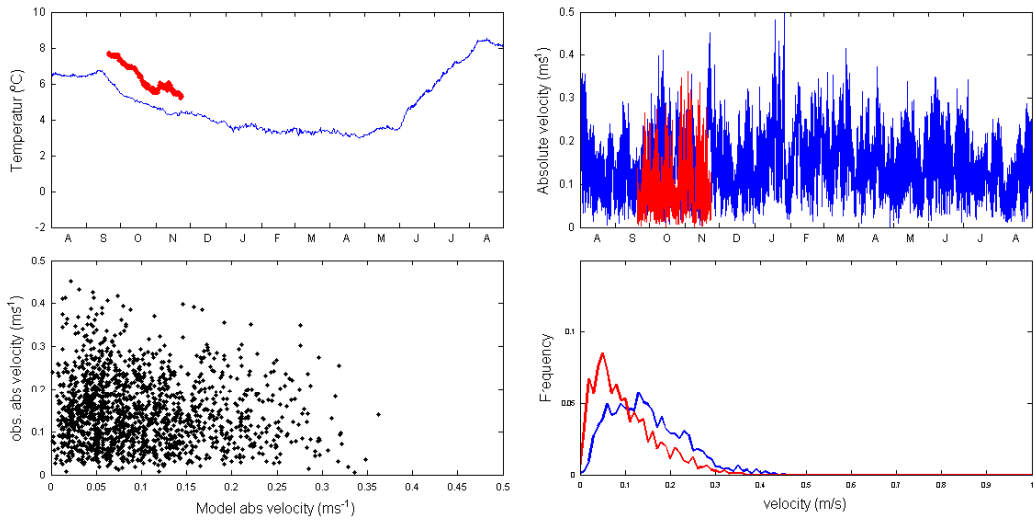
Pos: 31.0017; 72.5039

Direction frequency



Dir. mass transport



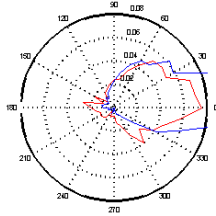


Rig: Barfn6

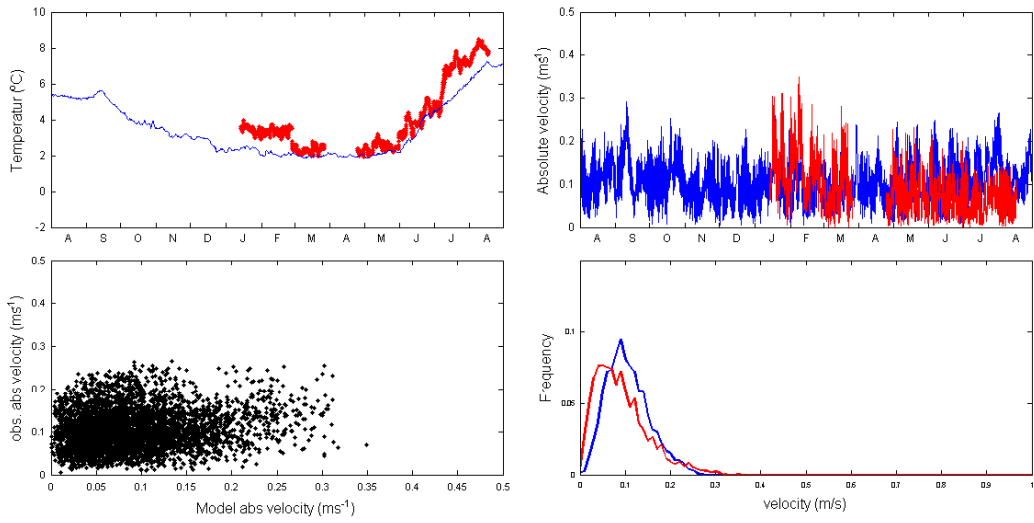
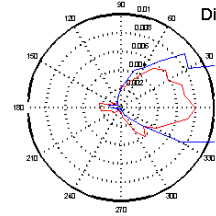
Depth: 003

Pos: 31.0083; 73.0056

Direction frequency



Dir. mass transport

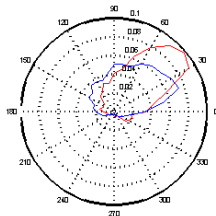


Rig: Barhe1

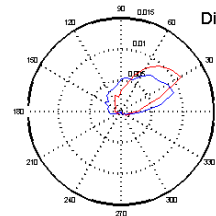
Depth: 003

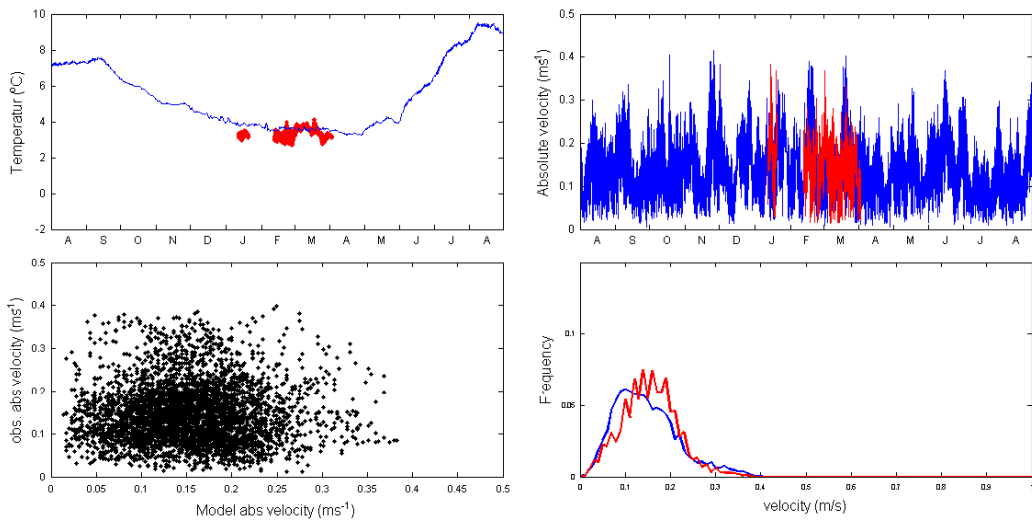
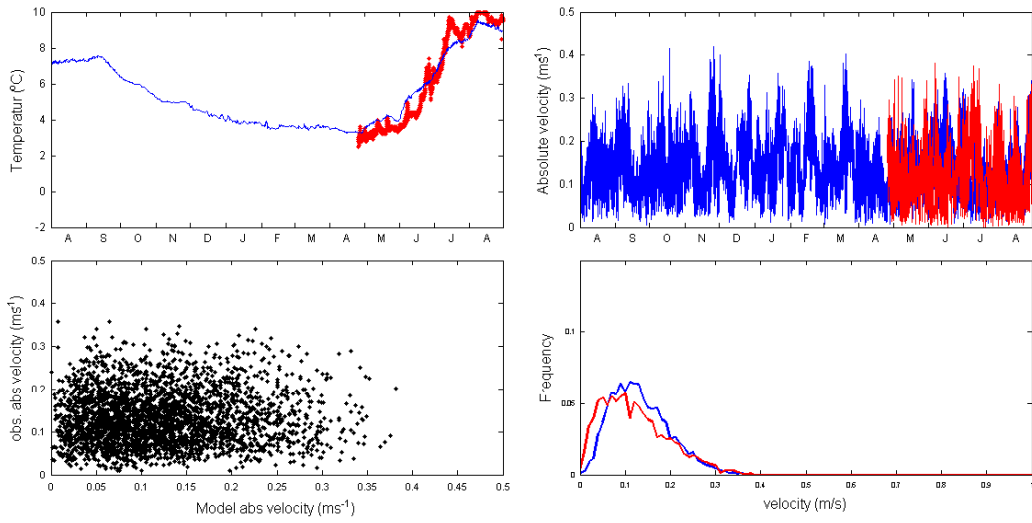
Pos: 29.7342; 74.3367

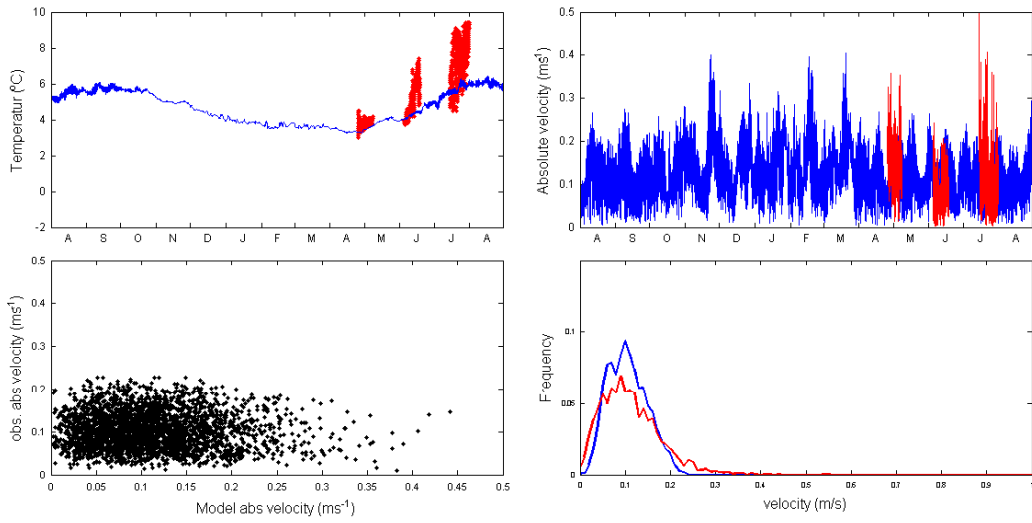
Direction frequency



Dir. mass transport





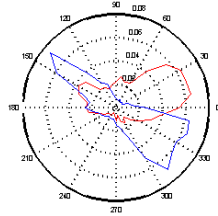


Rig: Barhn1

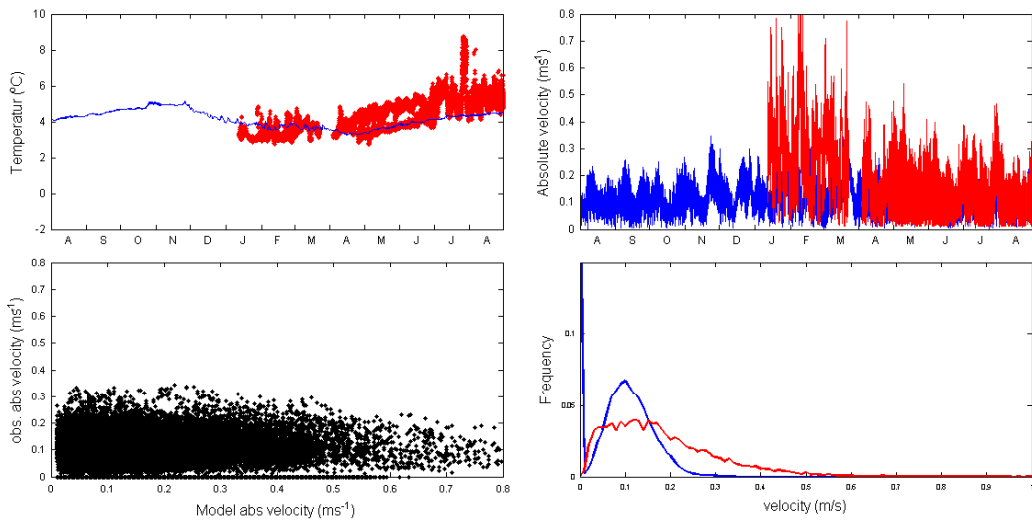
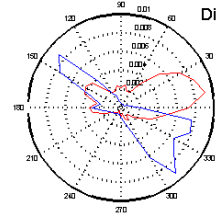
Depth: 025

Pos: 31.0444; 72.0000

Direction frequency



Dir. mass transport

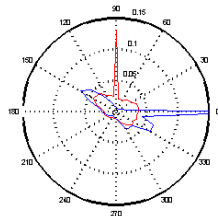


Rig: Barhn1

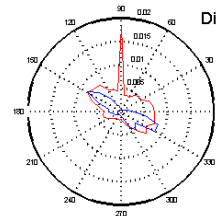
Depth: 050

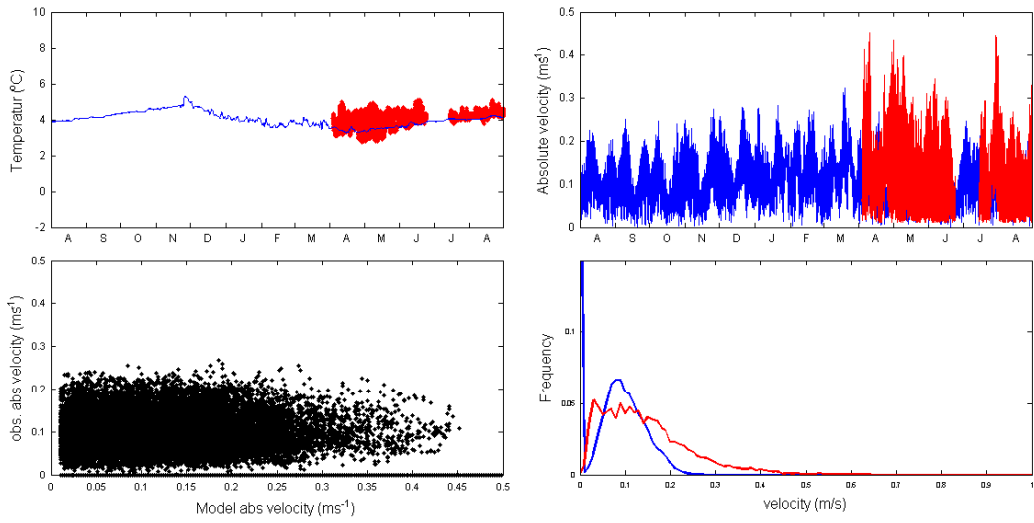
Pos: 31.0147; 72.0000

Direction frequency



Dir. mass transport



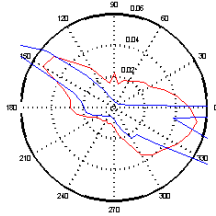


Rig: Barfn1

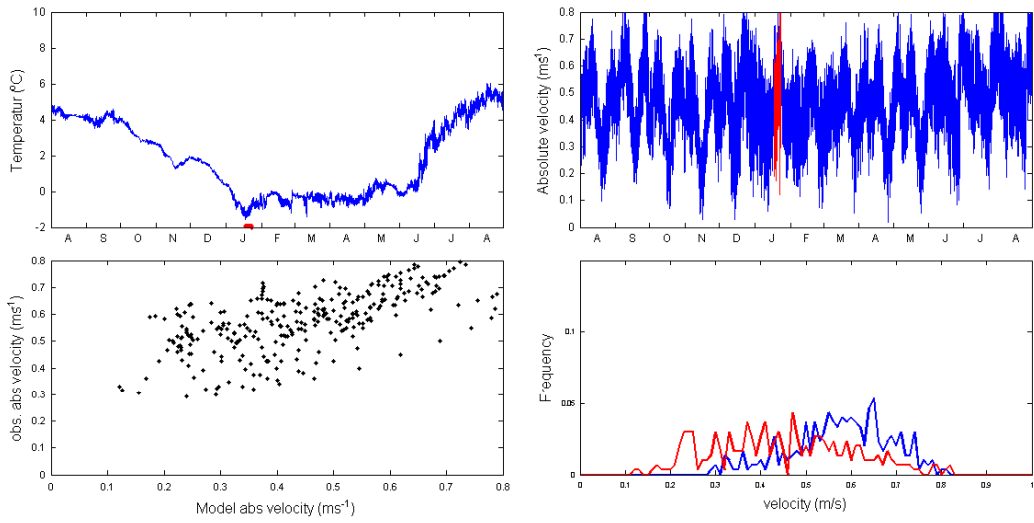
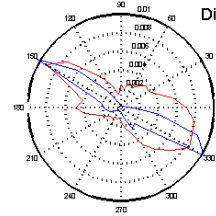
Depth: 100

Pos: 31.0147; 72.0000

Direction frequency



Dir. mass transport

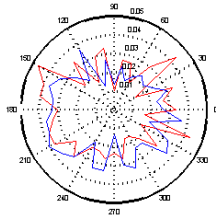


Rig: Barfs1

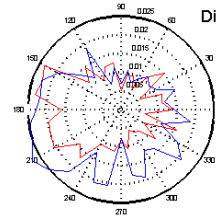
Depth: 010

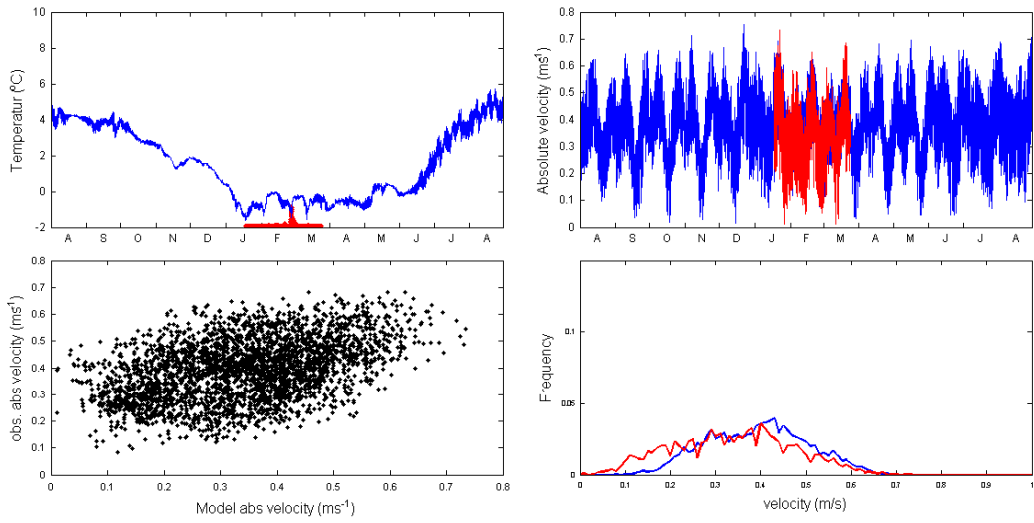
Pos: 21.2547; 75.0069

Direction frequency



Dir. mass transport



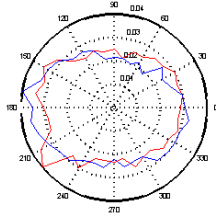


Rig: Barhs1

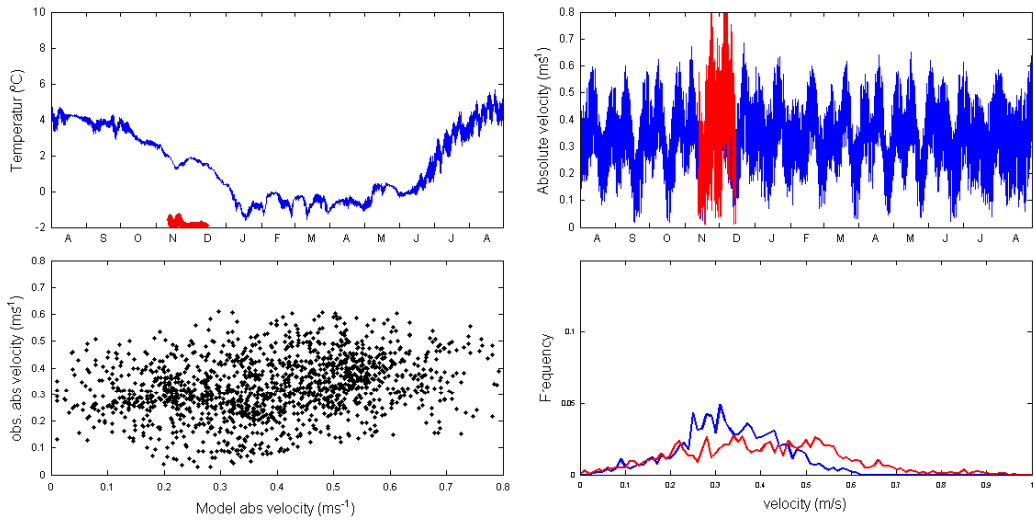
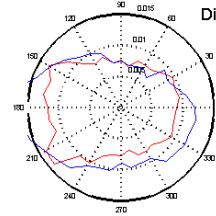
Depth: 025

Pos: 21.2547; 75.0069

Direction frequency



Dir. mass transport

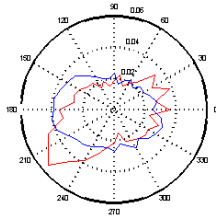


Rig: Barhs1

Depth: 033

Pos: 21.9544; 75.6789

Direction frequency



Dir. mass transport

